energies

MDPI

Article

Induction Motor Supplied with Voltage Containing Symmetrical Subharmonics and Interharmonics

Piotr Gnaciński [1,*], Damian Hallmann [1], Adam Muc [2], Piotr Klimczak [3] and Marcin Pepliński [1]

[1] Department of Ship Electrical Power Engineering, Gdynia Maritime University, 83 Morska St., 81-225 Gdynia, Poland
[2] Department of Ship Automation, Gdynia Maritime University, 83 Morska St., 81-225 Gdynia, Poland
[3] Diagnostic and Service of Electric Motors Department, Zakład Maszyn Elektrycznych EMIT Cantoni Group, 72 Narutowicza St., 99-320 Żychlin, Poland
* Correspondence: p.gnacinski@we.umg.edu.pl

Abstract: Sinusoidal voltage fluctuations can be considered a specific result of the occurrence of voltage subharmonics and interharmonics, which are components of low frequency or not being an integer multiple of the frequency of the fundamental voltage harmonic. These components—symmetrical subharmonics and interharmonics—are of the same magnitude, while their frequencies are symmetrical with respect to the fundamental frequency. Depending on their phase angles, various kinds of voltage fluctuations can be distinguished: amplitude modulation, phase modulation and intermediate modulation. In this study, the effect of phase angles on noxious phenomena in induction motors was analyzed. Additionally, torque pulsations and vibrations of an induction motor under sinusoidal voltage fluctuation and a single voltage subharmonic or interharmonic were compared. The investigations were performed with the finite element method and an experimental method. Among other findings, it was found that for some phase angles torque pulsations could be about ten times higher than for other angles, roughly corresponding to the amplitude modulation.

Keywords: AC motors; harmonic distortion; induction motors; vibrations; voltage fluctuations

Citation: Gnaciński, P.; Hallmann, D.; Muc, A.; Klimczak, P.; Pepliński, M. Induction Motor Supplied with Voltage Containing Symmetrical Subharmonics and Interharmonics. *Energies* **2022**, *15*, 7712. https://doi.org/10.3390/en15207712

Academic Editor: Frede Blaabjerg

Received: 9 September 2022
Accepted: 14 October 2022
Published: 19 October 2022

1. Introduction

A widely used industrial prime mover is a cage induction motor. Two of its most important advantages are reliability and durability. However, adverse working conditions, such as for example the occurrence of significant power quality disturbances, may result in its premature destruction [1–3]. A common power quality disturbance is a voltage waveform distortion connected with the presence of undesirable components in the supply voltage—usually harmonics. Other harmful components that may exist in the voltage waveform are interharmonics and subharmonics. The former are defined as components of the frequency that are not an integer multiple of the frequency of the fundamental harmonics. The latter are components of the frequency less than the fundamental harmonics. Subharmonics are often regarded as a kind of interharmonics (subsynchronous interharmonics), although in some works (e.g., [4–7]) they are considered separately because of their specific impact on electrical equipment [8]. In this study, subsynchronous components are referred to as subharmonics, and supersynchronous ones as interharmonics.

Subharmonics and interharmonics (*SaIs*) originate from the work of non-linear and pulsating loads [8–15] as well as renewable sources of energy [8,14–19]. *SaIs* can also be present in the output voltage of inverters [6,7,12,20]. In some power systems, voltage *SaIs* may reach a comparatively high level [11,18,21]. For example, ref. [11] reported the following voltage *SaIs* occurring together: a voltage subharmonic of frequency 45 Hz, value 0.9% and voltage interharmonics of frequencies 135 Hz, 225 Hz, 405 Hz and values 1.17%, 0.89% and 0.931%, respectively. The *SaI* contamination appeared in the 60 Hz

system, powered from diesel-driven generators, and it was caused by the work of inverters supplying high power induction motors.

A specific case of the simultaneous presence of *SaIs* is sinusoidal voltage fluctuations [8,22–25]. The voltage waveform contains two additional components of the same magnitude, while their frequencies are equal to the frequency of the fundamental harmonic (f_1) ± the frequency of voltage fluctuations (f_f) [8,22–25]. For instance, for the voltage fluctuations of a 10 Hz frequency in a 50 Hz system, the voltage waveform contains *SaIs* of 40 Hz and 60 Hz frequencies. Considering [22] (where they were called symmetrical interharmonics), in this study such couples of *SaIs* are referred to as symmetrical subharmonics and interharmonics (*SSaIs*). It should be noted that, depending on their phase angles [8,22], various kinds of voltage fluctuations can occur: amplitude modulation (*AM*), phase modulation (*PhM*) and intermediate modulation.

SaIs are considered an extraordinarily harmful power quality disturbance. They exert a detrimental impact on light equipment, power and measurement transformers, control systems, electronic power appliances and rotating machinery [4,8,12,22,26]. In induction motors, they cause a local saturation of the magnetic circuit, an increase in power losses, overheating, speed fluctuations [6,7,23–25,27–35] and torque pulsations [20,30–32] that can induce [2,3] excessive vibration [5,9]. To make the matter worse, the frequency of torque pulsation may correspond to the natural frequency of the first elastic-mode of the rotating mass [20,31,32]. Under elastic-mode resonance, torque pulsations may be significantly amplified [20,36], which can cause a mechanical failure of a power train [20,31,32]. Such a case was analyzed in [20]. Namely, the fluctuations of the inverter output voltage resulted in pulsations of the electromagnetic torque of a value merely 1.5% (peak-to-peak) of the design motor torque. In the wake of elastic-mode resonance, they were augmented by a factor of 110, which induced coupling destruction.

In spite of the extraordinary harmfulness of *SaIs*, their permissible values generally have not been introduced into power quality standards and regulations. According to the standard EN 50,160 voltage characteristics of electricity supplied by public distribution systems [37], "Levels are under consideration, pending more experience". Further, in the standard IEEE-519: *IEEE Recommended Practices and Requirements for Harmonic Control in Electric Power Systems* [38], only limits based on lamp flicker are included in an informative annex. As per the standard [38], due consideration should be given to the effect of interharmonics on various types of electrical equipment, including motors.

The previous works concerning the effect of voltage *SaIs* on induction motors were generally restricted to either the perfect *AM* [23,27–30] or a single subharmonic/interharmonic component occurring in the voltage waveform [5,26,31–35]. The exceptions are [24,25], in which currents and speed fluctuations were analyzed for both the above cases. The appropriate calculations were performed by employing the dq transformation. The presented results of the investigations showed that the local maxima of current subharmonics, current interharmonics and speed fluctuations could be significantly lower for the *AM* than for the injection of single voltage subharmonics.

It should be stressed that phase angles and possible interaction of current *SaIs* under voltage fluctuations were not taken into consideration in the previous works. At the same time, these issues could be especially important during the analysis of an induction motor. This is so because symmetrical voltage subharmonics and voltage interharmonics result in current components and torque pulsations of the same frequencies. For example, let us consider voltage *SSaIs* of frequencies 40 Hz and 60 Hz, occurring in a 50 Hz system. The voltage subharmonic of frequency f_{sh} = 40 Hz causes the flow of *SaIs* currents of frequencies 40 Hz, 60 Hz and torque pulsations of frequency f_p = 10 Hz, exactly as voltage interharmonic of frequency f_{ih} = 60 Hz. Consequently, for some phase angles torque pulsations and *SaIs* currents (caused separately by voltage subharmonic and voltage interharmonic) are expected to supercharge, and for other angles, to weaken. It is also worth mentioning that in the previous papers the effects of the *AM*, *PhM* and a single voltage

subharmonic/interharmonic on torque pulsations and vibration of induction motors were not compared.

The main purpose of this work is to point out that phase angles significantly affect undesirable phenomena occurring in the induction motor under voltage *SSaIs*, and in some cases their values are almost as important as the values of voltage subharmonics and interharmonics. Additionally, a comparison of torque pulsations and vibrations caused by sinusoidal voltage fluctuations and a single voltage subharmonic/interharmonic is presented. The investigations were carried out with the finite element method and an experimental method.

The structure of this article is as follows. Sections 2 and 3 describe voltage fluctuations and an analytical model of an induction motor. Section 4 presents the methodology. Sections 5–7 provide the results of the research on currents, torque pulsations and vibrations. Section 8 concludes this study.

2. Voltage Fluctuations

Voltage fluctuations occur in various power systems, both land and marine [8,39] and are considered as one of the most common and critical power quality issues (based on [8,23,40,41]). The fluctuations are usually defined as fast changes in the rms voltage value [8,40,42]. However, under voltage fluctuations the amplitude as well as the phase can be modulated [8].

In the conditions of voltage fluctuations, the instantaneous voltage value can be described as (based on [8,43])

$$v(t) = V_{1A}[1 + m_v(t)]\cos[2\pi f_1 t + \varphi_v(t)] \quad (1)$$

where V_{1A} and f_1 are the amplitude and the frequency of the fundamental voltage component, $m_v(t)$ and $\varphi_v(t)$ are functions modulating the amplitude and the phase.

Let us assume that phase angle φ_1 of the fundamental component $V_{1A}\cos(2\pi f_1 t + \varphi_1)$ is null and that the frequency of voltage fluctuations is less than f_1. For the perfect amplitude or phase modulation, (1) takes the forms (based on [8,23,40,42]):

$$v(t) = V_{1A}[1 + m_v(t)]\cos(2\pi f_1 t) \quad (2)$$

$$v(t) = V_{1A}\cos[2\pi f_1 t + \varphi_v(t)]. \quad (3)$$

A specific case of voltage fluctuations is a sinusoidal modulation of the amplitude and the phase, which can be described as (based on [43]):

$$v(t) = V_{1A}[1 + k_v\cos(2\pi f_m t + \phi_v)] \times \cos\left[2\pi f_1 t + k_{ph}\cos\left(2\pi f_m t + \phi_{ph}\right)\right] \quad (4)$$

where k_v and k_{ph} are the factors describing the depth of modulation, f_m is the modulation frequency, ϕ_v and ϕ_{ph} are phase angles of the modulating function.

For the assumption that the sine of a small angle is equal to its value (expressed in radians), the cosine is equal to unity and after omitting some negligible frequency components, it can be pointed out (based on [8]) that the sinusoidal modulation (4) may be considered as the superposition of the fundamental voltage component and *SSaIs* [8,22,23]:

$$v(t) = V_{1A}[\cos(2\pi f_1 t) + a\cos(2\pi f_{sh} t + \phi_{sh}) + a\cos(2\pi f_{ih} t + \phi_{ih})] \quad (5)$$

where a is the value of voltage *SSaIs*, related to the fundamental voltage harmonic, for the *AM* a is equal to $k_v/2$, and for the *PhM*—$k_{ph}/2$, ϕ_{sh} and ϕ_{ih} are phase angles, f_{sh}, f_{ih} are frequencies of subharmonic and interharmonic components, equal to:

$$f_{sh} = f_1 - f_m \quad (6)$$

$$f_{ih} = f_1 + f_m. \quad (7)$$

Note that for the assumed phase angle $\phi_1 = 0^\circ$, angles ϕ_{sh} and ϕ_{ih} are evaluated with reference to the cosines of frequencies f_{sh}, f_{ih} and of null phase angles at $t = 0$ [22]. Additionally, for the assumption that the frequency of voltage fluctuations is lower than f_1,

both the subharmonic and interharmonic components are of the positive sequence (based on [15]). For the voltage waveform described with (5), the *AM* occurs if $\phi_{sh} + \phi_{ih} = 0°$, while the *PhM* occurs if $\phi_{sh} + \phi_{ih} = 180°$ [22]. Exemplary waveforms of *SSaIs* and their superposition with the fundamental component are presented in Figures 1 and 2. The former corresponds to phase angles equal to $\phi_{sh} = 0°$, $\phi_{ih} = 0°$ (*AM*) and the latter—to $\phi_{sh} = 0°$, $\phi_{ih} = 180°$ (*PhM*).

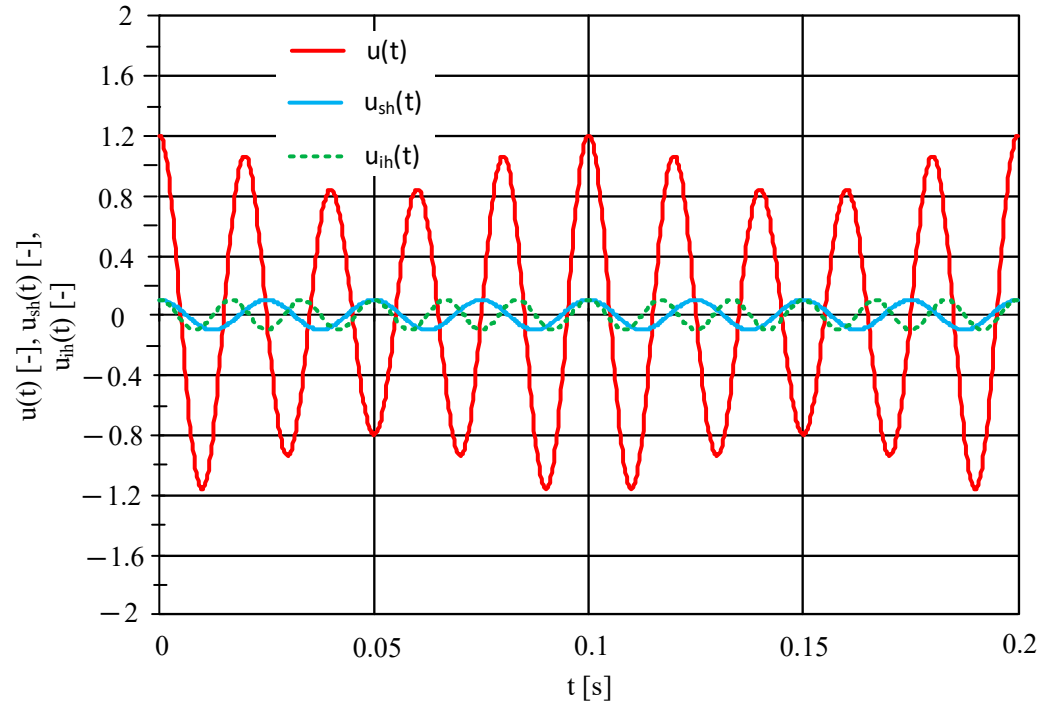

Figure 1. Subharmonic and interharmonic components and their superposition with the fundamental component for $a = 0.1$, $f_{sh} = 40$ Hz, $f_{ih} = 60$ Hz and $\phi_{sh} = 0°$, $\phi_{ih} = 0°$ (amplitude modulation).

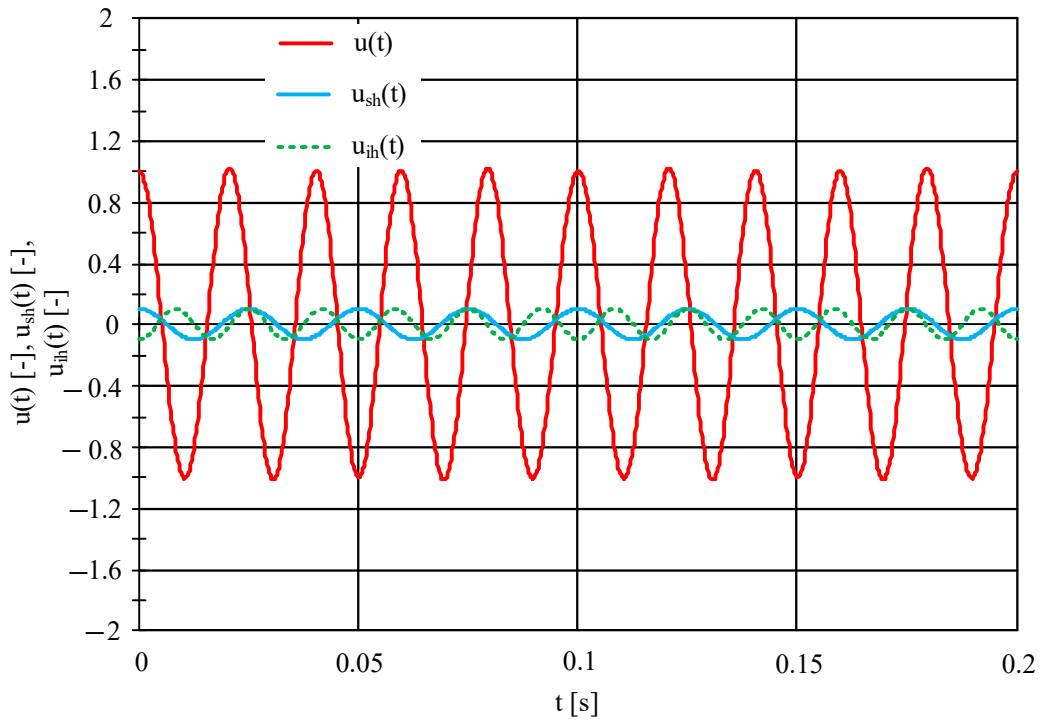

Figure 2. Subharmonic and interharmonic components and their superposition with the fundamental component for $a = 0.1$, $f_{sh} = 40$ Hz, $f_{ih} = 60$ Hz and $\phi_{sh} = 0°$, $\phi_{ih} = 180°$ (phase modulation).

It is worth adding that even the perfect *PhM* results in little amplitude volatility, the maximal per-unit value of which is [22]:

$$\delta_v = \sqrt{1 + (2a)^2} - 1. \tag{8}$$

The main reason for voltage fluctuations is current variation [8]. For the current modulation described with (9) [8]:

$$i(t) = \sqrt{2} I_0 [1 + m_i(t)] \cos[2\pi f_1 t - \psi + \varphi_i(t)] \tag{9}$$

where I_0 is the rms value of the non-fluctuating current component, $m_i(t)$ and $\varphi_i(t)$ are functions modulating the amplitude and the phase, ψ is the phase angle, the function modulating the voltage amplitude and the phase can be expressed as [8]:

$$m_v(t) = -(RP_0 + XQ_0)m_i(t) + (XP_0 - RQ_0)\varphi_i(t) - LP_0\frac{dm_i}{dt} - LQ_0\frac{d\varphi_i}{dt} \tag{10}$$

$$\varphi_v(t) = (RQ_0 - XP_0)m_i(t) - (XQ_0 + RP_0)\varphi_i(t) - LQ_0\frac{dm_i}{dt} + LP_0\frac{d\varphi_i}{dt} \tag{11}$$

where R and X are per-unit fundamental-frequency source impedances, L is per-unit source inductance, P_0 and Q_0 are per-unit non-fluctuating active and reactive power.

For the slow current modulation:

$$f_m \ll \frac{f_1}{\frac{X}{R}} \tag{12}$$

(in the case of the sinusoidal modulation), (10) and (11) take the form [8]:

$$m_v(t) = -(RP_0 + XQ_0)m_i(t) + (XP_0 - RQ_0)\varphi_i(t) \tag{13}$$

$$\varphi_v(t) = (RQ_0 - XP_0)m_i(t) - (XQ_0 + RP_0)\varphi_i(t). \tag{14}$$

The above equations show that even the perfect amplitude or phase modulation in current causes both the *AM* and the *PhM* in voltage [8]. At the same time, voltage fluctuations are usually considered as the *AM* (based on [42]). As the *PhM* is not expected to result in excessive flickers (based on [22]), this approach is validated for the assessment of their severity. In the case of the induction motor, the assumption that voltage fluctuations are limited to the perfect *AM*, de facto results in the motor analysis for phase angles $\phi_{sh} + \phi_{ih} = 0^\circ$, while their real values may considerably differ.

3. Analytical Model of Induction Motor under Voltage Fluctuations

Various methods can be used for the analysis of induction motors; for example, they can be based on a transformer-type equivalent circuit, the dq transformation and a dedicated equivalent circuit.

The simplest method employs a transformer-type equivalent circuit [34]. The method is characterized by simplicity of computations and comparatively high accuracy (based on the authors' experience, for example [34]). Its main drawback is the omission of speed fluctuations, which consequently causes that the use of this method to be limited. In the case of positive sequence subharmonics [15], it can be applied only for motors driving a load with a high inertia moment [34]. For an exemplary 3 kW motor investigated in [34], the load's moment should be at least three times greater than the motor's moment. For the lower load moment of inertia, the application of this method may result in an unacceptable computational error.

Speed fluctuations are included in the method based on the dq transformation, which is widely used to examine electrical machinery. For modeling the induction motor under *SaIs*, the synchronously rotating reference frame is usually applied (for example [24,25,34]). A detailed description of this method is provided in [24,25]. Its disadvantage is the omission of non-linear phenomena appearing in the induction motor.

Ghaseminezhad et al. [27] elaborated and experimentally verified another method that makes use of a dedicated equivalent circuit (Figure 3). The circuit consists of three

parts, constituting coupled circuits for the fundamental, interharmonic and subharmonic components (respectively, the upper, middle and lower part of Figure 3). The appropriate couplings are possible due to the presence of additional electromotive sources depending on voltages, which are denoted in Figure 3 as V_x, V_{xih}, V_{xsh}. The circuits together with couplings correspond to the following equations (based on [27]):

$$V_1 = \left(R_S + j2\pi f_1 L_S + L_S \frac{d}{dt}\right) I_{S1} + \left(j2\pi f_1 L_M + L_M \frac{d}{dt}\right) I_{R1} \tag{15}$$

$$\begin{aligned} 0 = &\left(j2\pi f_1 L_M + L_M \tfrac{d}{dt}\right) I_{S1} + \left[R_R + \left(j2\pi f_1 L_R + L_R \tfrac{d}{dt}\right)\right] I_{R1} \\ &- j\Omega_{R0}(L_M I_{S1} + L_R I_{R1}) - j\Omega_{Rm}(L_M I_{Ssh} + L_R I_{Rsh}) \\ &- j\Omega_{Rm}(L_M I_{Sih} + L_R I_{Rih}) \end{aligned} \tag{16}$$

$$V_{ih} = \left(R_S + j2\pi f_{ih} L_S + L_S \frac{d}{dt}\right) I_{Sih} + \left(j2\pi f_{ih} L_M + L_M \frac{d}{dt}\right) I_{Rih} \tag{17}$$

$$\begin{aligned} 0 = &\left(j2\pi f_{ih} L_M + L_M \tfrac{d}{dt}\right) I_{Sih} + \left[R_R + \left(j2\pi f_{ih} L_R + L_R \tfrac{d}{dt}\right)\right] I_{Rih} \\ &- j\Omega_{R0}(L_M I_{Sih} + L_R I_{Rih}) - j\Omega_{Rm}(L_M I_{S1} + L_R I_{R1}) \end{aligned} \tag{18}$$

$$V_{sh} = \left(R_S + j2\pi f_{sh} L_s + L_S \frac{d}{dt}\right) I_{Ssh} + \left(j2\pi f_{sh} L_M + L_M \frac{d}{dt}\right) I_{Rsh} \tag{19}$$

$$\begin{aligned} 0 = &\left(j2\pi f_{sh} L_M + L_M \tfrac{d}{dt}\right) I_{Ssh} \\ &+ \left[R_R + \left(j2\pi f_{sh} L_R + L_R \tfrac{d}{dt}\right)\right] I_{Rsh} - j\Omega_{R0}(L_M I_{Ssh} + L_R I_{Rsh}) \\ &- j\Omega_{Rm}(L_M I_{S1} + L_r I_{R1}) \end{aligned} \tag{20}$$

where L_M is mutual inductance, Ω_{R0} and Ω_{Rm} are the average angular speed and the amplitude of speed fluctuations due to voltage fluctuations, subscripts S, R refer to a stator and a rotor, respectively, and subscripts 1, *sh* and *ih* to the fundamental, subharmonic and interharmonic components.

The above equations show how voltage subharmonics induce current interharmonics due to speed fluctuations and vice versa. Of note, if the speed fluctuations are neglected (for example, for high load moment of inertia), the circuits become three separate transformer-type equivalent schemes for the fundamental, subharmonic and interharmonic components.

In the above methods, the presence of stator and rotor slots is neglected. In the next method, developed by Ghaseminezhad et al. [29], this is taken into account during the magnetic analysis. The calculation results show a good correlation with the experimental and numerical data. According to [29], this method can be applied for optimization, the assessment of the life expectancy of mechanical components and studies on vibrations.

Apart from the analytical methods, field methods are commonly used to investigate induction motors under voltage fluctuations as well, to analyze the generation of *SaIs* by electrical machinery driving a fluctuating load [9]. The applied field model is presented in the next section.

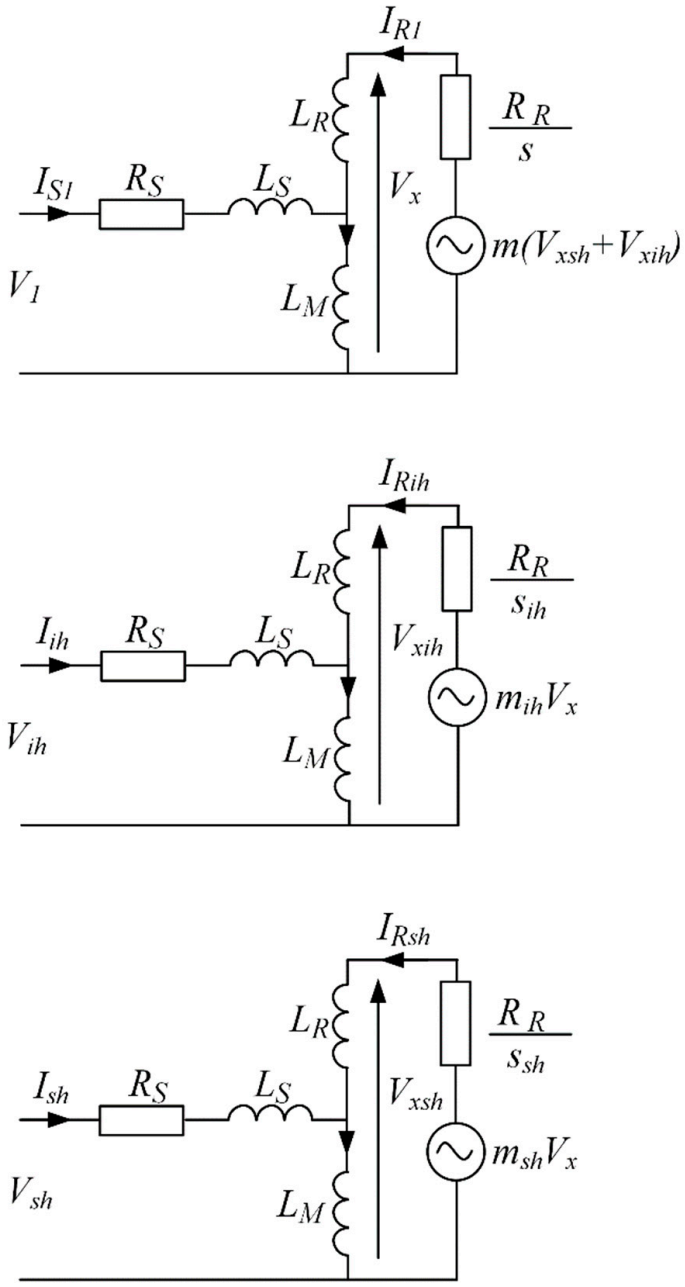

Figure 3. Dedicated equivalent circuit for the analysis of an induction motor under voltage fluctuations; s_{sh} is a slip for the subharmonic component; s_{ih} is the slip for the interharmonic component; V_1, V_{sh} and V_{ih} are the fundamental, subharmonic and interharmonic voltage components; m, m_{ih}, m_{sh} are auxiliary variables depending on the amplitude of speed fluctuations, the modulation frequency, the fundamental frequency and the rotational speed.

4. Methodology

Currents and torque pulsations under voltage *SaIs* were investigated with the finite element method (*FEM*), and vibration with an experimental method.

Numerical computations were carried out for cage induction motors, type SLgm 315 ML2B (200 kW) and TSg100L-4B (3 kW), referred to in this study as motor1 and motor2. Their name plate parameters are presented in Table 1. During the 2D *FEM* analysis, the ANSYS Electronics Desktop environment (ANSYS Electromagnetics Suite 18.0.0) and the MAXWELL-ANSYS environment were employed. The appropriate calculations were performed with a transient-type solver for tau-type meshes. For motor1 this consisted of

8082 triangle elements, and for motor2, of 22,094 elements. The maximal side dimensions of the finite elements are specified in [32,33]. Of note, ANSYS Electromagnetics Suite 18.0.0 was also used to calculate current *SaI* for motor1, while for motor2 a separate application was employed, generally in compliance with the standard [44]. The parameters of the supply voltage, including phase angles of *SSaIs*, were set in the used environments.

Table 1. Name plate data of the investigated motors.

Motor	Motor1	Motor2	Motor3
Type	SLgm 315 ML2B	TSg100L-4B	3SIE100L4B
Rated power (kW)	200	3	3
Rated frequency (Hz)	50	50	50
Rated voltage (V)	400	380	400
Rated current (A)	335	6.9	6.3
Rated power factor (-)	0.90	0.81	0.79
Rated rotational speed (rpm)	2982	1415	1465

The model parameters were determined on the basis of the construction data and the results of empirical tests [32,33]. It is worth mentioning that one of the co-authors is an employee of the manufacturer of motor1 (Zakład Maszyn Elektrycznych EMIT S.A. Cantoni Group) and took part in the design process of the motor. A comprehensive description of the applied *FEM* models is provided in [31–34], together with the experimental verification for motor 2 (motor1 was not tested experimentally under *SaIs* because of its high rated power).

For the experimental research, a laboratory setup was used, composed of two 3 kW induction motors, a vibration measurement system, a computer power quality analyzer and a programmable power source. Two investigated motors, type 3SIE100L4B, (see Table 1) were attached to a rigid frame. One of them was uncoupled and the other coupled with the DC generator (Figure 4). In this study, they are referred to as motor3 Case A and motor3 Case B, respectively. For the vibration measurements the Bruel&Kjear (B&K) system was applied. It consisted of a standalone four-channel data acquisition module (B&K type: 3676-B-040), a three-axis accelerometer (B&K type: 4529-B of the following parameters: frequency range: 0.3–12,800 Hz, weight: 14.5 g, sensitivity: 10 mV/ms^{-2}, maximum shock level peak: 5100 g) with a calibrator (B&K type: 4294) and a computer equipped with the BK Connect software. The accelerometer was mounted to a steel stand (Figure 4) screwed to a motor casing made of cast aluminum. It is worth adding that the accelerometer was calibrated before each measurement and that the experimental investigations were carried out generally in accordance with the main provisions of the standards [44,45]. In particular, the vibration measurements were taken simultaneously in three axes. For each measurement point, the accelerometer indications were recorded three times. Based on statistical metrics such as the mean value, standard deviation, etc., the acceleration waveforms were evaluated to select the most appropriate one. The chosen waveform was passed through a low-pass filter and then converted into vibration velocity. Of note, the broad-band velocity [45] is required by the standards [45,46] for the assessment of vibration severity. A flowchart of the measurement procedure is presented in Figure 5.

The motors under consideration were supplied with an AC programmable power source type Chroma 61512+A615103, of the rated power 36 kVA. It enabled injection of a single subharmonic or interharmonic component into the output voltage and setting the voltage *AM*. Because of the limitations of the power source, the sinusoidal-shape function modulating voltage could not be set directly, but it was approximated with line segments. Exemplary spectra of the testing voltage are shown in Figure 6. They were determined with two methods: the computational (theoretical) method, and on the basis of the measurements of the voltage produced by the AC power source loaded with the investigated motor. Both the spectra show sufficient consistency.

The simplified diagram of the measurement stand is presented in Figure 7 (based on [31]).

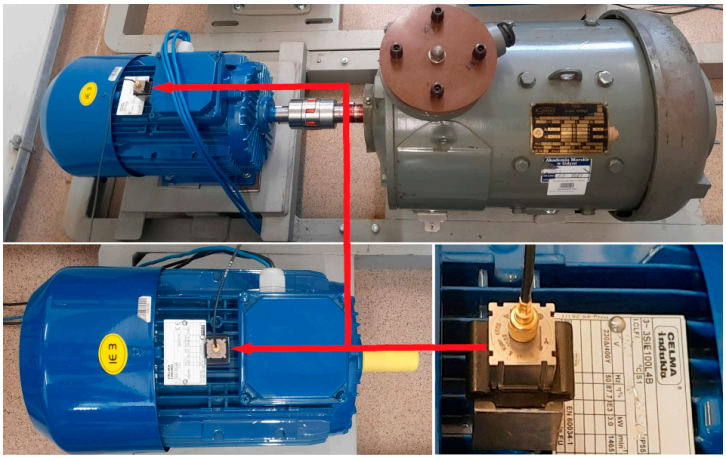

Figure 4. Motor3 Case B (**top**), motor3 Case A (**bottom left**) and the accelerometer (**bottom right**).

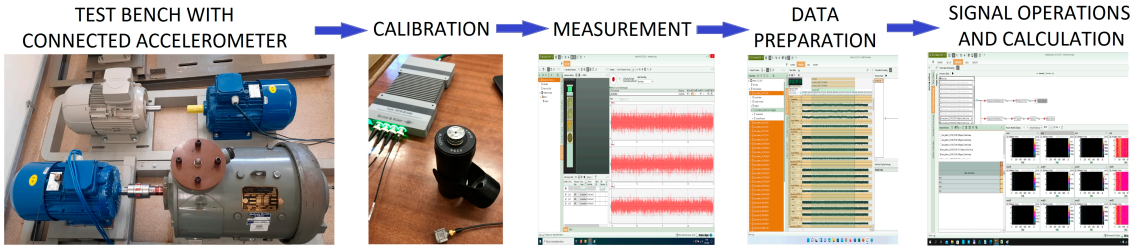

Figure 5. Flowchart of the vibration measurement.

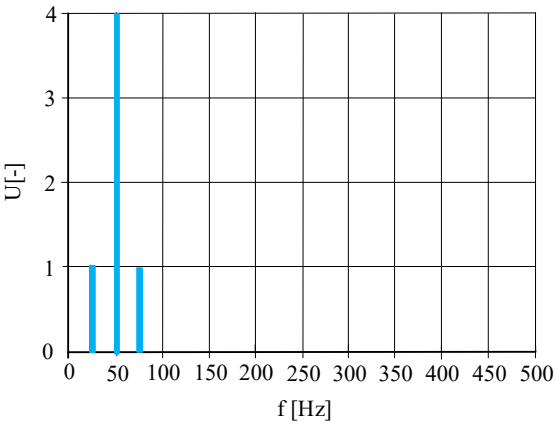

(**a**)

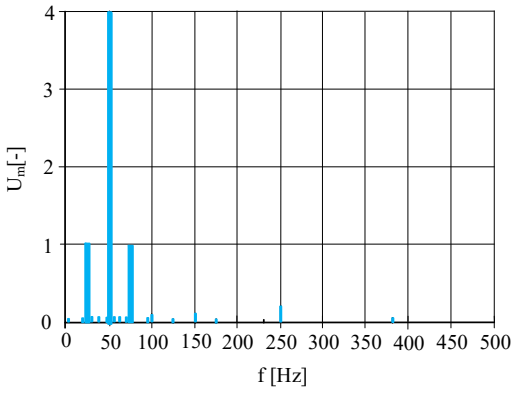

(**b**)

Figure 6. Spectrum of the voltage waveform for frequency f_m = 25 Hz: (**a**) determined with the calculations and (**b**) the measured output from the programmable power source.

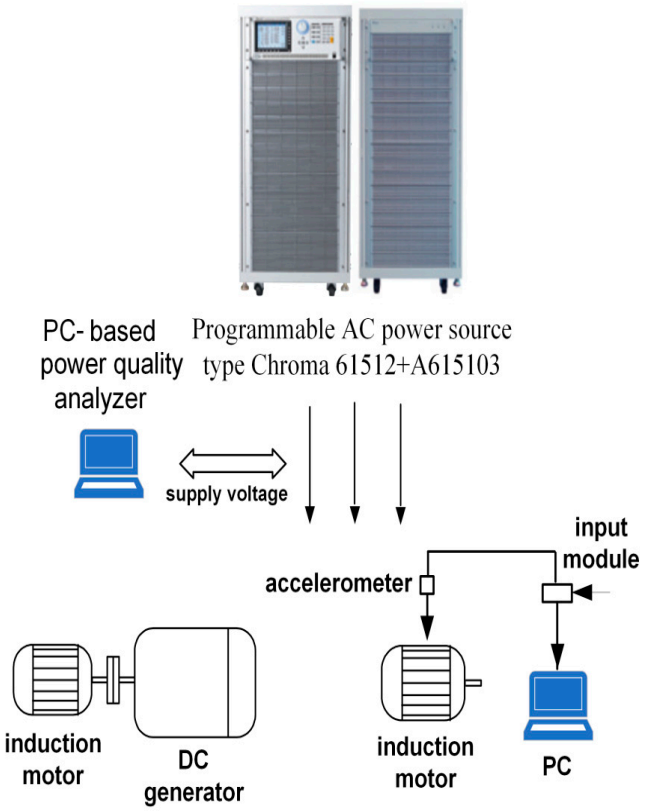

Figure 7. Simplified diagram of the measurement stand.

5. Effect of *SSaIs* on Current

This section presents the effects of voltage fluctuations on current *SaIs*. As the load moment of inertia has a significant impact on undesirable phenomena occurring in an induction motor under voltage *SaIs* [31,32,34], the *FEM* computations were performed for two extreme cases: a load with a negligible moment of inertia and the work with a constant rotational speed. In practice, the constant rotational speed corresponds to the work with the load moment of inertia much greater [34] than the motor's moment. The numerical experiments were carried out for the load torque and the fundamental voltage components equal to the rated values, the angle $\phi_{sh} = 0^\circ$ and voltage *SaIs* equal to 1%. It is worth adding that, in all the presented diagrams, the rms values of current *SaI* refer to the rated currents of the investigated motors.

In order to present the properties of the induction motor under voltage *SaIs*, Figure 8 shows the waveforms of electromagnetic torque, rotational speed and stator current for motor2, $f_m = 20$ Hz, $\phi_{ih} = 0^\circ$, a negligible load moment of inertia and a step change of load torque from 0 to 100%. The fluctuations in the electromagnetic torque, speed and current result from the *SaIs* influence and non-linear phenomena occurring in the induction motor [23,32,34,47–49]. Transients of induction motors under *SaIs* will be the subject a separate study.

In the next diagram (Figure 9), the current *SaIs* versus the angle ϕ_{ih} are presented for the modulation frequency f_m corresponding to rigid-body resonance [9,23,32]. If the frequency of torque pulsations f_p (based on [25]):

$$f_p = f_m = f_1 - f_{sh} \tag{21}$$

$$f_p = f_m = f_{ih} - f_1. \tag{22}$$

is close to the natural frequency of the rigid-body mode of rotating mass (f_{Nrb}) [9,23,32], the speed fluctuations caused by torque pulsations boost current *SaIs*, which increases torque pulsations and speed fluctuations even more. Consequently, at the rigid-body resonance,

extraordinarily high speed fluctuations and current *SaIs* may occur. For motor1 and motor2, the frequencies f_m corresponding to the rigid-body resonance (determined on the grounds of field computations) are 7 Hz and 30 Hz, respectively. Of note, the rigid-body resonance occurs only for motors driving loads with a comparatively low moment of inertia [34] and for this reason it is not the case for the constant rotational speed.

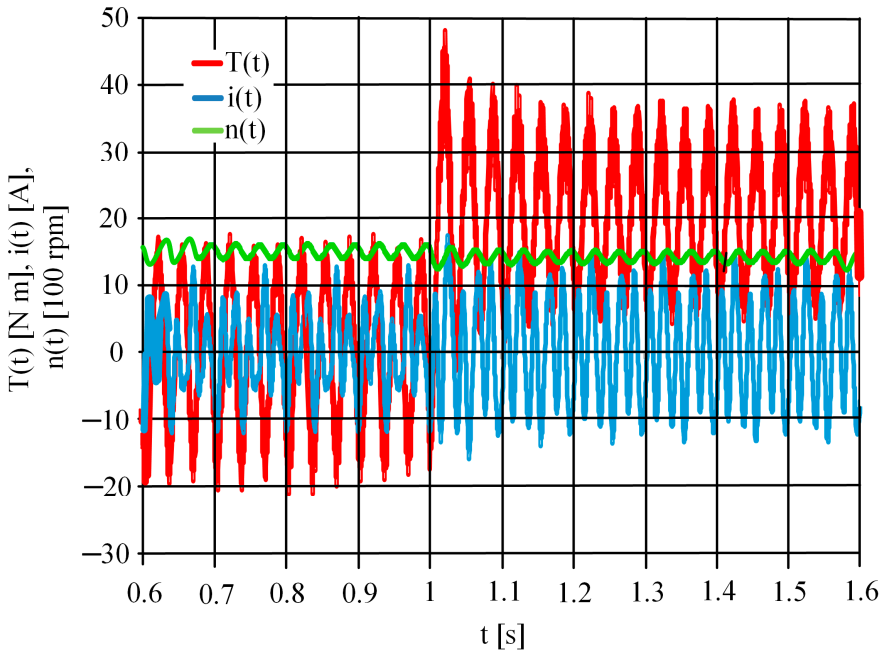

Figure 8. Electromagnetic torque, rotational speed and stator current waveforms for motor2, f_m = 20 Hz, ϕ_{ih} = 0°, a negligible load moment of inertia and a step change of load torque from 0 to 100% of T_{rat}.

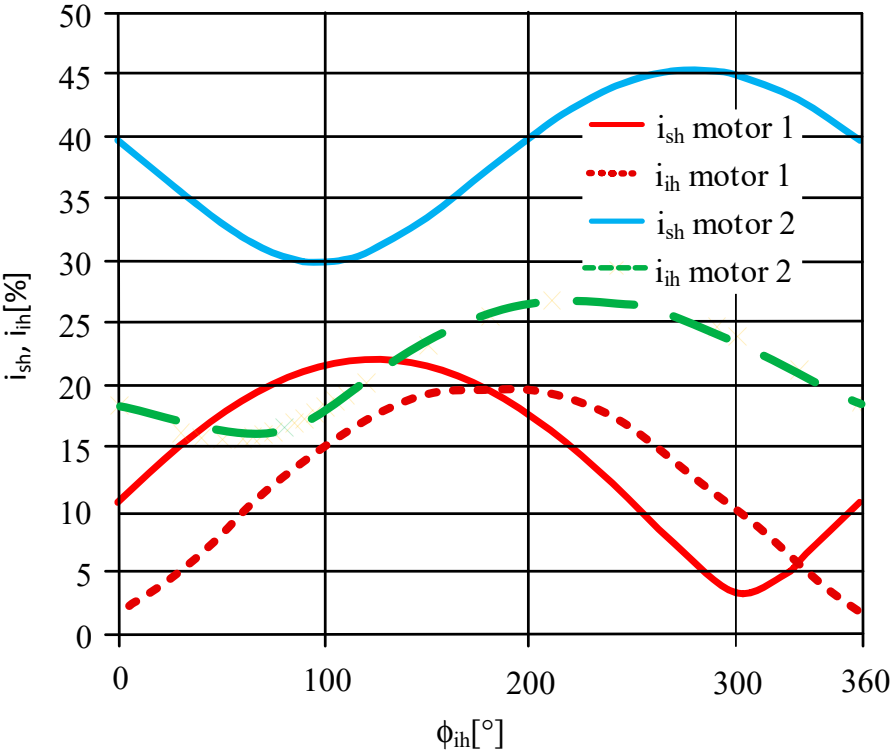

Figure 9. Current subharmonics and interharmonics versus the angle ϕ_{ih} for ϕ_{sh} = 0°, the load with a negligible moment of inertia and voltage fluctuation of the resonant frequency equal to f_m = 7 Hz and f_m = 30 Hz for motor1, motor2, respectively.

The characteristics provided in Figure 9 show that current *SaIs* significantly depend on the angle ϕ_{ih}. For motor1, the maximal and minimal values of current subharmonics are 22.1% of I_{rat} and 3.3% of I_{rat} for the angles $\phi_{ih} \approx 120^\circ$ and $\phi_{ih} \approx 300^\circ$. Further, current interharmonics (*CIs*) reach the maximum and the minimum for $\phi_{ih} \approx 180^\circ$ and $\phi_{ih} \approx 0^\circ$, respectively, and the corresponding values are 19.7% of I_{rat} and 1.6% of I_{rat}. It should be noted that, for this case, the *CIs* caused independently by voltage subharmonics and voltage interharmonics are of similar values (10.6% and 9.1% of I_{rat}). Additionally, for $\phi_{ih} \approx 0^\circ$ they are of the opposite phase. For this reason, they cancel each other out. On the contrary, for $\phi_{ih} \approx 180^\circ$ the *CIs* caused independently by voltage subharmonics and voltage interharmonics are of the same phase and add up algebraically. Consequently, their maximal value in Figure 9 is about twice as high as for a single-voltage subharmonic or interharmonic. Further, for motor2 (Figure 9), current *SaIs* are less affected by the angle ϕ_{ih} than for motor1. Current *SaIs* reach the minima for the angles ϕ_{ih} approximately equal to 100° and 50°, and the maxima for 280° and 230°. The next diagram (Figure 10) presents the analogous characteristics as in Figure 9, but determined for the constant rotational speed. For both the motors, the angle ϕ_{ih} has rather a moderate effect on current *SaIs*. Of note, in Figures 9 and 10 current subharmonics take considerably higher values for motor2 than for motor1.

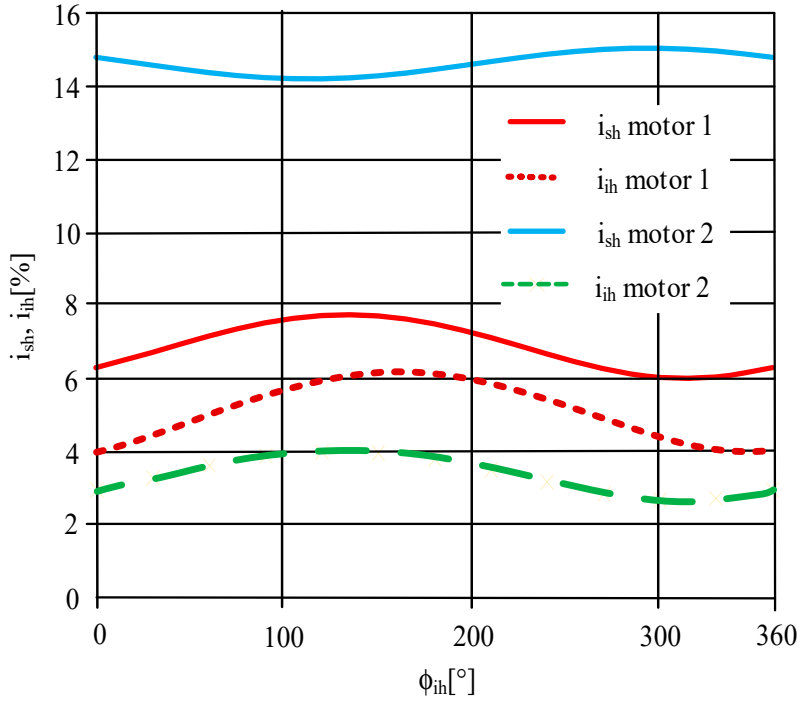

Figure 10. Current subharmonics and interharmonics versus the angle ϕ_{ih} for $\phi_{sh} = 0^\circ$, the work with a constant rotational speed, voltage fluctuation of the frequency equal to f_m = 7 Hz and f_m = 30 Hz for motor1, motor2, respectively.

The calculated current *SaIs* versus the frequency of the voltage modulation f_m are given in Figures 11–14. Figures 11 and 12 correspond to the load with a negligible moment of inertia, and Figures 13 and 14 to the constant rotational speed. For motor1 and the load with a negligible moment of inertia, current *SaIs* under the *PhM* (Figure 12) are up to above ten times higher than for the *AM* (Figure 11), while for the constant rotational speed (Figures 13 and 14) the differences are less significant. It should be noted that medium and high power induction motors are characterized by relatively low values of winding resistance and the frequency f_{Nrb} [32], which explains the shape of the considered characteristics. Peaks of current result from the presence of the above-mentioned rigid body resonance. Similar peaks were observed in [5,24,25,27,31,32,34]. For example, in [27] the *AM* of depth k_v = 5% and the frequency f_m close to 30 Hz caused an increase in the rms value of the stator current from about 2.5 A to c. 3.2 A. It is also worth mentioning that for motor1 the *PhM*

(Figures 12 and 14) results in significantly greater current subharmonics (up to about 55%) than a single voltage subharmonic (see [32]). Further, for motor2, current subharmonics are of comparable values for both the cases of modulation, while current interharmonics are generally considerably higher for the *PhM* than the *AM* (up to c. 50%).

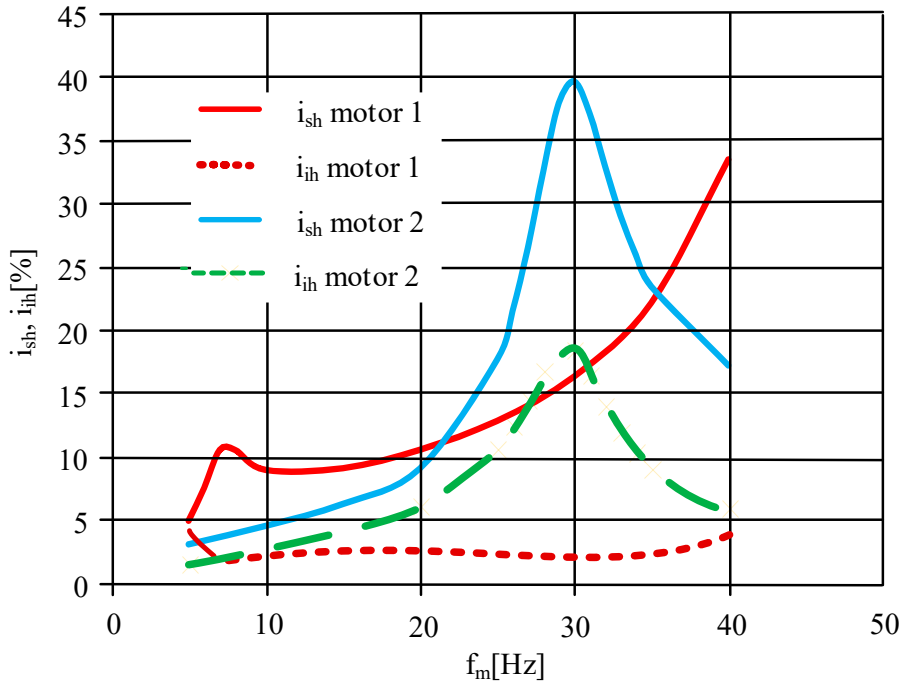

Figure 11. Current subharmonics and interharmonics versus the frequency of voltage fluctuations for the amplitude modulation ($\phi_{sh} = 0°$, $\phi_{ih} = 0°$) and the load with a negligible moment of inertia. The frequency components are related to the rated current.

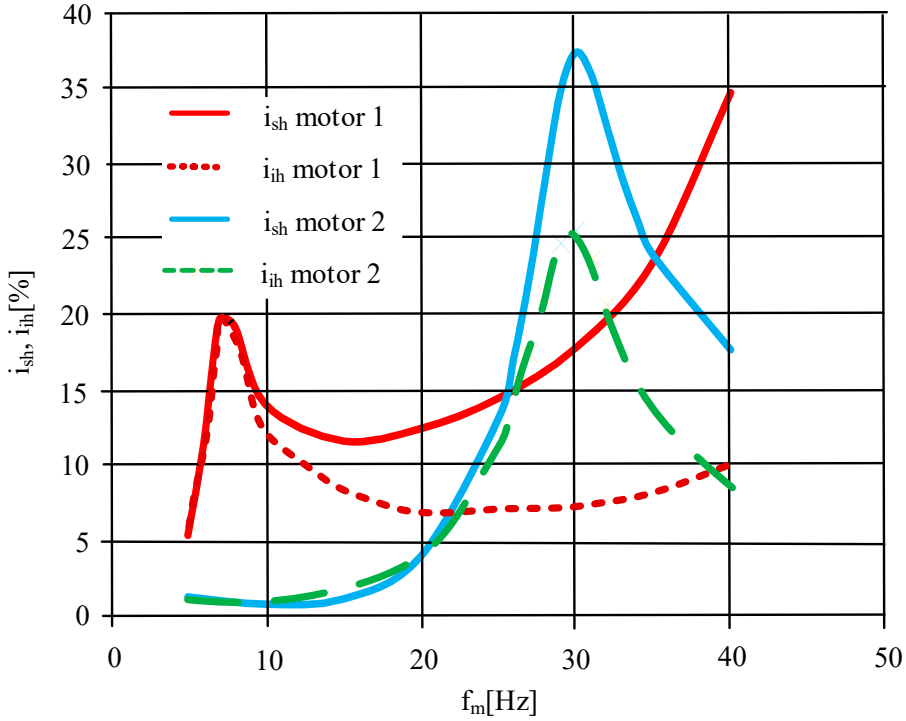

Figure 12. Current subharmonics and interharmonics versus the frequency of voltage fluctuations for the phase modulation ($\phi_{sh} = 0°$, $\phi_{ih} = 180°$) and the load with a negligible moment of inertia. The frequency components are related to the rated current.

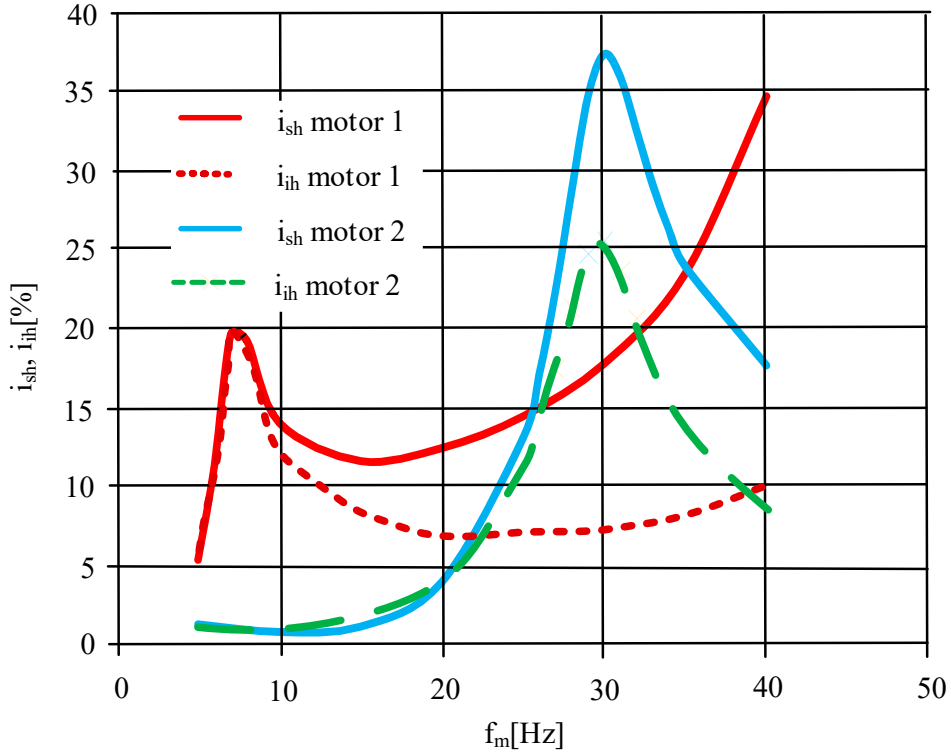

Figure 13. Current subharmonics and interharmonics versus the frequency of voltage fluctuations for the amplitude modulation ($\phi_{sh} = 0°$, $\phi_{ih} = 0°$) and the work with a constant rotational speed. The frequency components are related to the rated current.

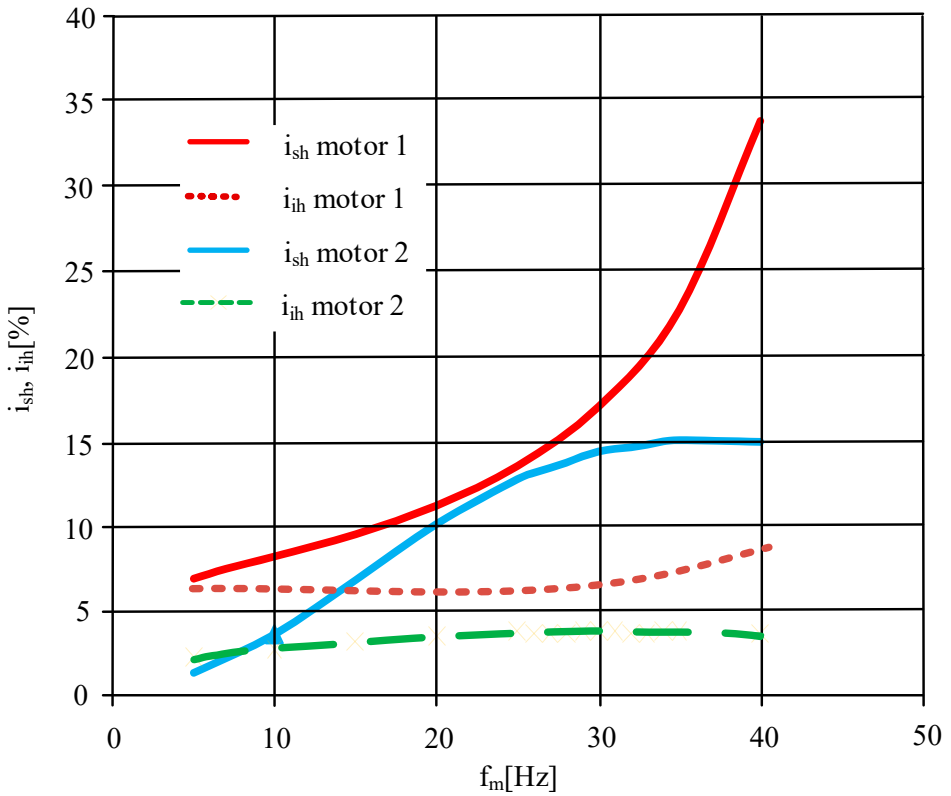

Figure 14. Current subharmonics and interharmonics versus the frequency of voltage fluctuations for the phase modulation ($\phi_{sh} = 0°$, $\phi_{ih} = 180°$) and the work with a constant rotational speed. The frequency components are related to the rated current.

In summary, the effect of sinusoidal voltage fluctuations on currents depend on the phase angles of *SSaIs*, especially at rigid-body resonance. For some phase angles, the impact of voltage subharmonics and voltage interharmonics adds up, which might lead to almost the duplication of current *SaIs* in comparison with their values caused by a single voltage subharmonic. Phase angles, for which the highest and the lowest current *SaIs* occur, differ for various motors. The detailed explanation of the observed phenomena will be the subject of future investigations.

6. Effect of *SSaIs* on Torque Pulsations

The most harmful effects of voltage *SaIs* on induction motors, such as vibration and torsional vibrations [5,20,23,31,32], are connected with torque pulsations [2,3,20]. The results of the investigations on torque pulsations caused by *SSaIs* are shown below. All the presented characteristics concern the pulsating torque component (ΔT_p) of the frequency described with (21), (22) and refer to the rated torques of the motors under investigation. The numerical experiments were performed for the same assumptions as in Section 5.

The characteristics of the pulsating torque component ΔT_p versus the angle ϕ_{ih} are provided in Figures 15 and 16 for frequency f_m = 7 Hz (motor1) and 30 Hz (motor1). As was mentioned in Section 4, these frequencies correspond to the rigid-body resonance. For the load with a negligible moment of inertia (Figure 15) and motor1, the pulsating torque component T_p reaches the maximum 44.3% of the rated torque (T_{rat}) for the angle $\phi_{ih} \approx 150°$. The minimal value is T_p = 5.0% of T_{rat} for $\phi_{ih} \approx 330°$. For motor2, the pulsating torque component T_p is significantly greater than for motor1. The maximal and minimal values of the component are 75.1% and 41.5% of T_{rat} and they occur for the angles $\phi_{ih} \approx 265°$ and $\phi_{ih} \approx 90°$, respectively. It is also worth adding that for both the motors the extrema of T_p appear for slightly bigger angles ϕ_{ih} than the extrema of current subharmonics and slightly lesser angles ϕ_{ih} than the extrema of current interharmonics (see Section 5).

As was pointed out in Section 5, for the constant rotational speed the phase angles have rather a moderate effect on current *SaIs*. However, the torque component ΔT_p shows considerable dependency on the angle ϕ_{ih} also for the constant rotational speed (Figure 16). The presence of the extrema in Figures 15 and 16 results from the fact that for some phase angles the torque component ΔT_p induced by voltage interharmonics adds to the component ΔT_p caused by voltage subharmonics, and for other phase angles it subtracts. It is worth adding that for the constant rotational speed the pulsating torque component ΔT_p reaches the extrema for the same angles ϕ_{ih} as for the load a with negligible moment of inertia (Figure 15).

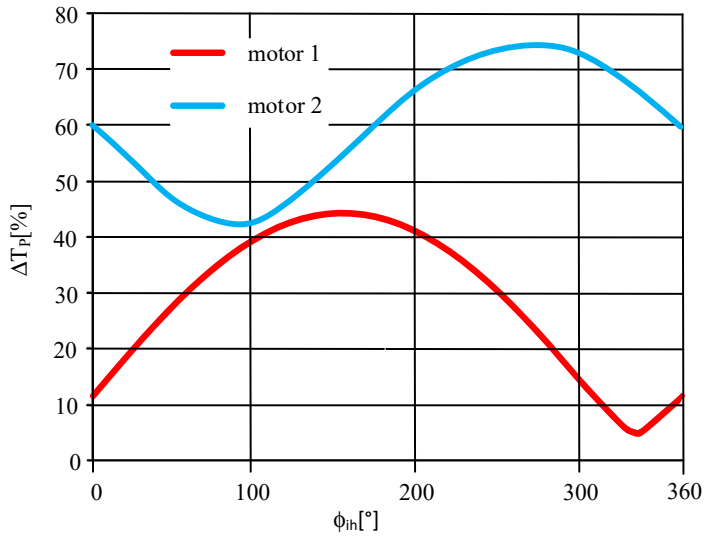

Figure 15. Pulsating torque component ΔT_p of the frequency described with (21), (22) versus the angle ϕ_{ih} for $\phi_{sh} = 0°$, the load with a negligible moment of inertia and voltage fluctuation of the resonant frequency equal to f_m = 7 Hz and f_m = 30 Hz for motor1, motor2, respectively.

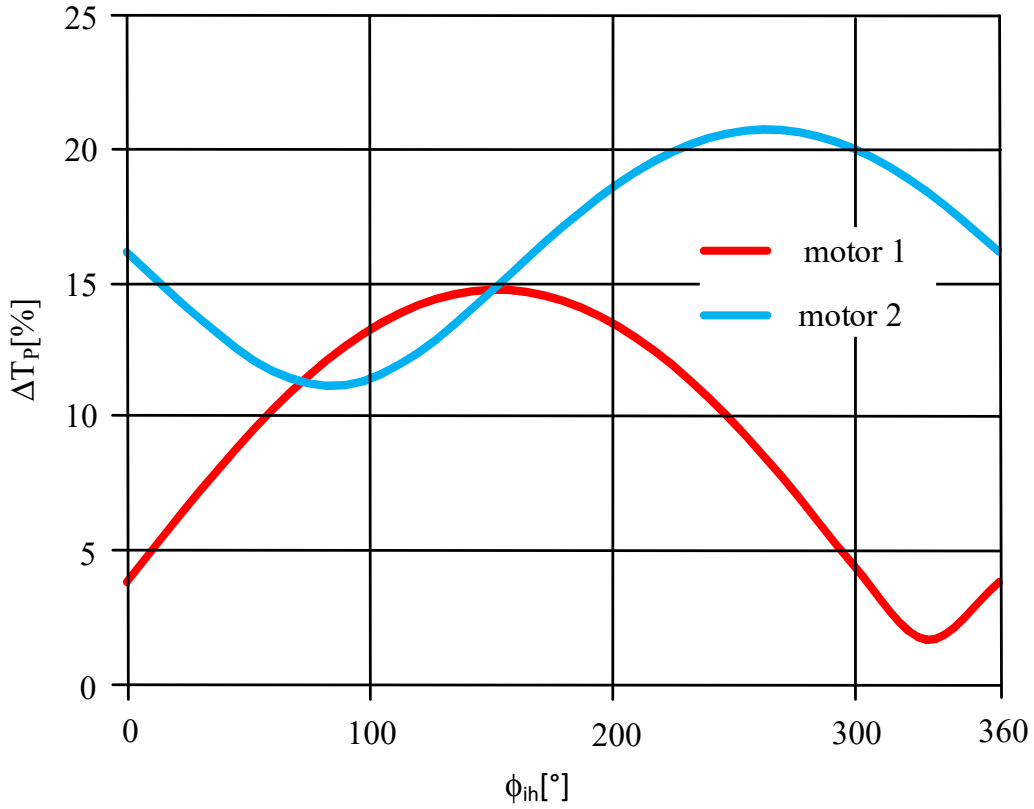

Figure 16. Pulsating torque component ΔT_p of the frequency described with (21), (22) versus the angle ϕ_{ih} for $\phi_{sh} = 0°$, the work with a constant rotational speed, voltage fluctuation of the frequency equal to $f_m = 7$ Hz and $f_m = 30$ Hz for motor1, motor2, respectively.

In the next diagrams (Figures 17 and 18) the characteristics of the pulsating torque component ΔT_p are given versus the frequency f_m for the *AM* ($\phi_{ih} = 0°$) and the *PhM* ($\phi_{ih} = 180°$). Additionally, the torque component ΔT_p due voltage subharmonic is shown in Figure 18 for informative purposes (the analogous characteristics for voltage interharmonics are presented in [31]). The peaks of the pulsating torque component occurring in the considered diagrams are caused by the rigid-body resonance (see the previous section). Similar peaks were observed in [27,31,32]. For an exemplary 1.1 kW motor under the *AM* of depth $k_v = 5\%$ and frequency f_m of about 30 Hz, the torque fluctuations reached the level comparable with the rated torque [27].

The results of computations presented in Figures 17 and 18 show that for motor1 the *PhM* leads to a considerably greater pulsating torque component ΔT_p than the *AM*. For both the considered cases—a load with a negligible moment of inertia and the constant rotational speed—the torque component ΔT_p under the *PhM* (Figure 18) is up to c. four times greater than for the *AM* (Figure 17). Further, for motor2 the pulsating torque component ΔT_p is of a similar value to the *AM* (Figure 17), *PhM* (Figure 18) as well as a single voltage subharmonic (Figure 19).

In summary, from the point of view of torque pulsation, phase angles are almost as important as the value of voltage *SSaIs*. For some phase angles, the pulsating torque component ΔT_p might be of an even greater order of magnitude than for the others.

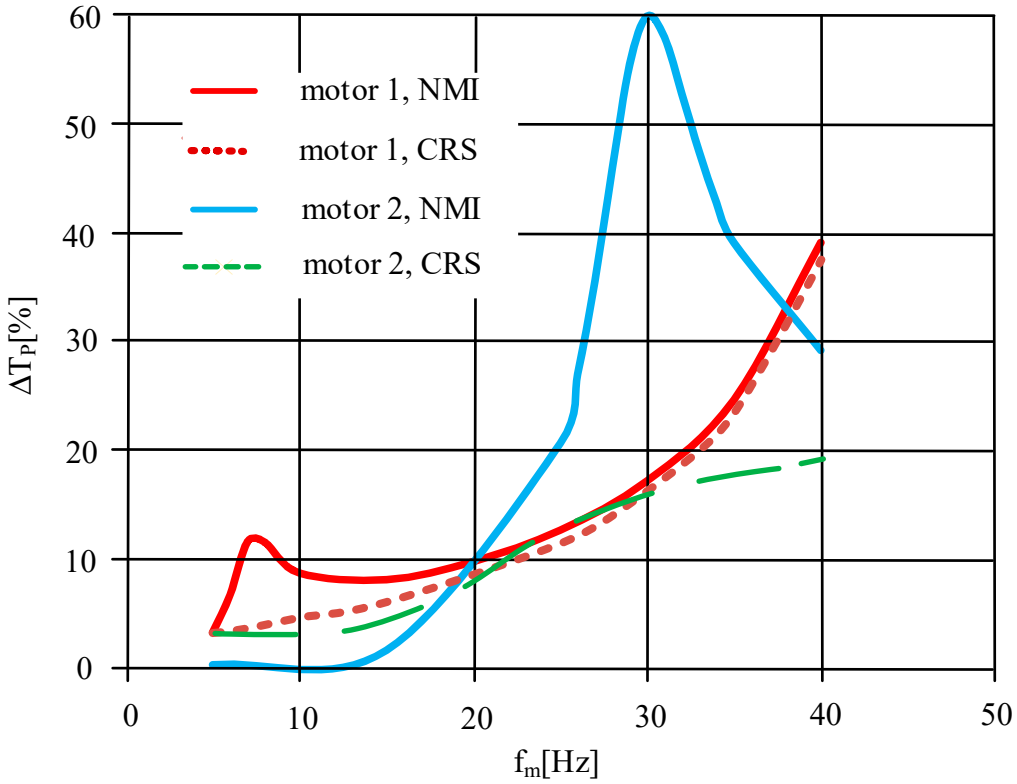

Figure 17. Pulsating torque component ΔT_p of the frequency described with (21), (22) versus the frequency of the voltage modulation for the amplitude modulation ($\phi_{sh} = 0°$, $\phi_{ih} = 0°$).

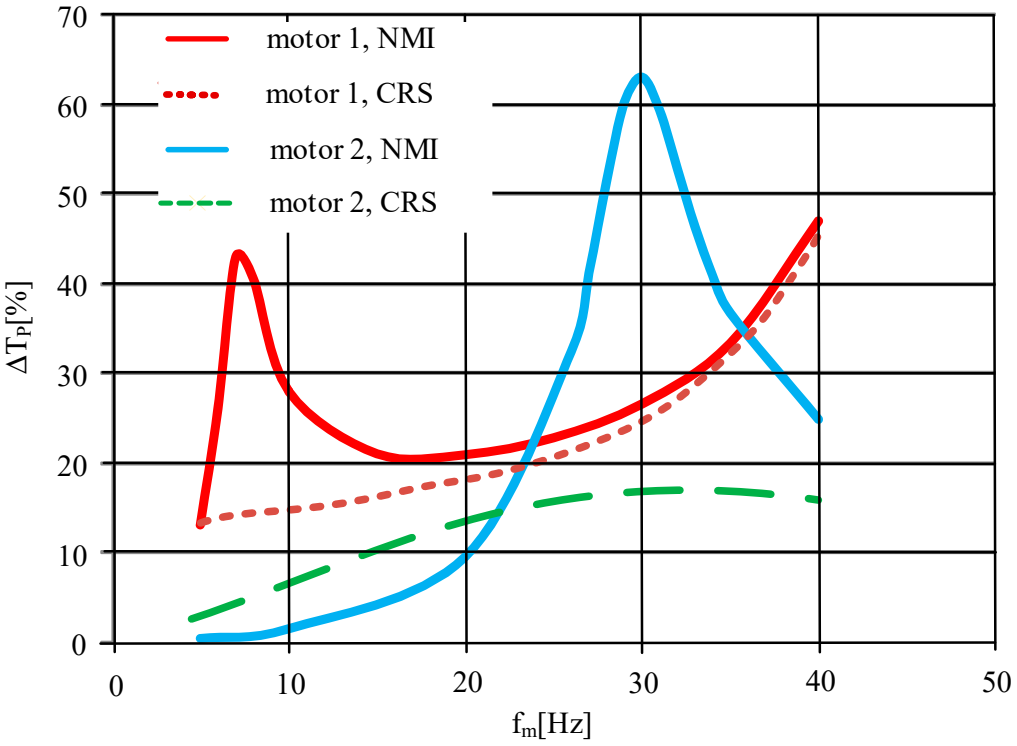

Figure 18. Pulsating torque component ΔT_p of the frequency described with (21), (22) versus the frequency of the voltage modulation for the phase modulation ($\phi_{sh} = 0°$, $\phi_{ih} = 180°$).

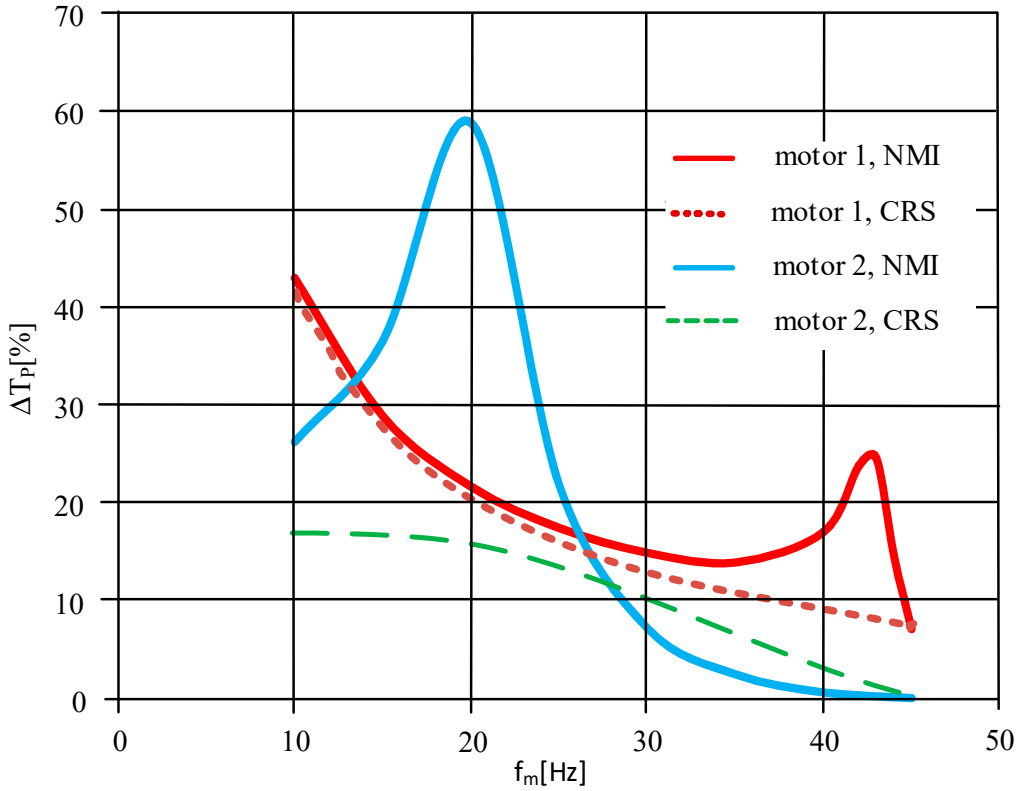

Figure 19. Pulsating torque component ΔT_p of the frequency described with (21), versus the frequency of voltage subharmonics occurring as a single power quality disturbance.

7. Effect of *SSaIs* on Vibration

According to the authors' experience [5,26,31], voltage *SaIs* cause the highest vibration for motors under no load. At the same time, some motors idle for most of their operational life, e.g., under the standard work S6 15% [50]. Therefore, the results of the measurements presented in this section concern no-load operation. The appropriate experimental investigations were carried out for motor3 and two cases: Case A, the uncoupled motor and Case B, the motor coupled with the unloaded DC generator (see Section 4). It should be noted that all the tests were carried out for voltage fluctuations of an amplitude equal to 2% or voltage *SaIs* of 1%. Because of the limitations of the used programmable power source (see Section 4), the measurements for the *PhM* and variable phase angles were not performed.

General guidelines concerning measurements and evaluation of vibration are included in the standards [45,46]. As the current standard ISO20816-1 Mechanical vibration—Measurement and evaluation of machine vibration—Part 1: General guidelines [45] does not contain the univocally specified recommendation concerning the assessment of vibration severity, for the purpose of this paper the recommendations included in its anterior version [46] were adopted.

The broad-band vibration velocity under the *AM* is provided in Figures 20 and 21 for Case A and Case B, respectively. Additionally, for informative purposes, Figures 22 and 23 present the measured current *SaIs*, while Figures 24 and 25 show vibration velocity for the supply voltage containing a single subharmonic or interharmonic. For Case A (Figure 20) the maximal value of vibration velocity is 6.67 mm/s for the modulation frequency f_m = 23 Hz, and for Case B (Figure 21) 6.80 mm/s for f_m = 35 Hz. It should be stressed that these vibration levels significantly exceed the threshold value of Zone D (4.5 mm/s [46]), defined in [45,46] for the evaluation of vibration severity. According to [45], the vibration within Zone D is normally considered to be of sufficient severity to cause damage to the machine [45]. For other frequencies f_m the vibration velocity is generally considerably lower, but it virtually exceeds the lower boundaries of another evaluation zone, Zone C. Vibrations within this zone (1.8 mm/s–4.5 mm/s [46]) are considered

unacceptable for long-term operation [45,46]. Of note for Case A, the vibration velocity (Figure 20) roughly corresponds to current *SaIs* caused by voltage fluctuations (Figure 22), while for Case B (Figures 21 and 23) the relevant characteristics differ significantly. It should be stressed that the vibration level is significantly affected by the behavior of the mechanical structure [2,3] and excessive motor electromagnetic vibration is very often a result of a resonance condition on the structure of an entire unit or on the motor components, such as a stator core or frame [2]. Further, the peaks appearing in Figures 20–24 can be explained by the occurrence of rigid body resonance (see the previous sections). It is also worth mentioning that the maximal vibration velocity under the *AM* approximately corresponds to the vibration velocity caused by a single subharmonic injection (Figures 24 and 25). For Case A, the maximal vibration velocity is 6.41 mm/s, while for Case B, 7.49 mm/s.

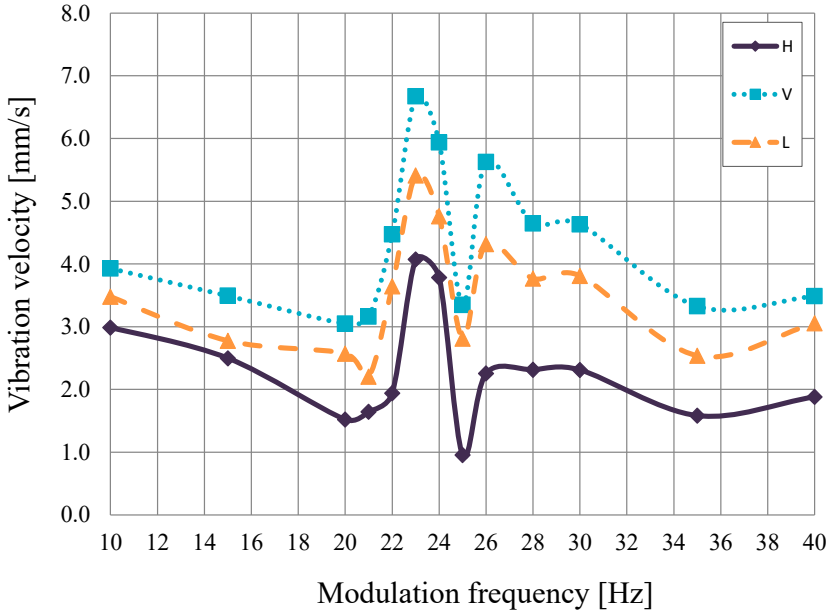

Figure 20. Measured broad-band vibration velocity for Case A in the horizontal (H), vertical (V) and longitudinal (L) directions versus the frequency of the voltage modulation.

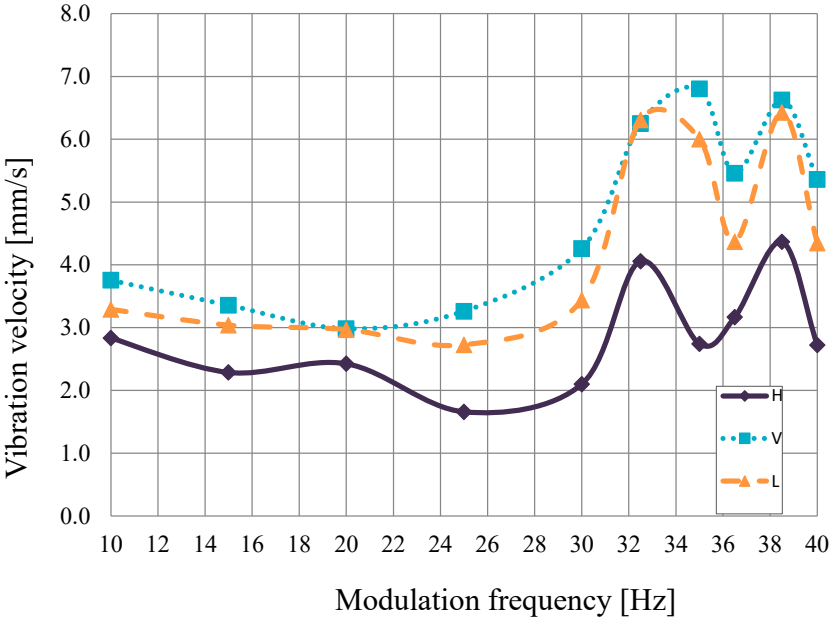

Figure 21. Measured broad-band vibration velocity for Case B in the horizontal (H), vertical (V) and longitudinal (L) directions versus the frequency of the amplitude modulation.

To sum up, the *AM* may cause significant vibration of velocity considerably exceeding the boundaries of evaluation Zone D [45,46]. For the investigated motor, both the *AM* and a single subharmonic injection result in a vibration of similar velocity.

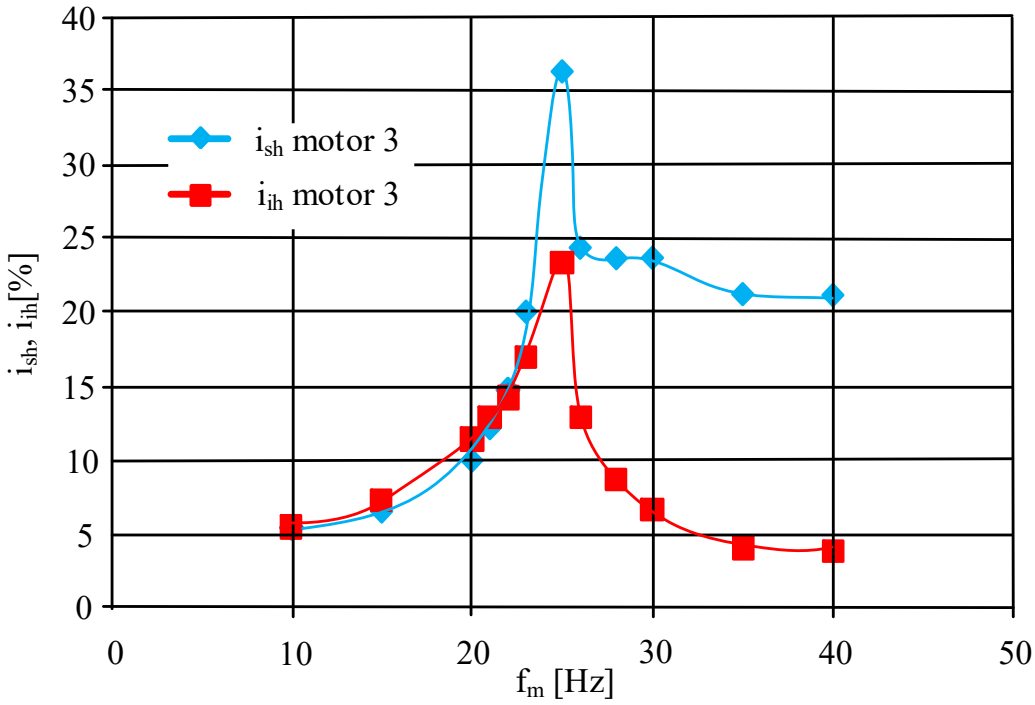

Figure 22. Measured current subharmonics and interharmonics versus the frequency of the amplitude modulation for Case A. The frequency components are related to the rated current.

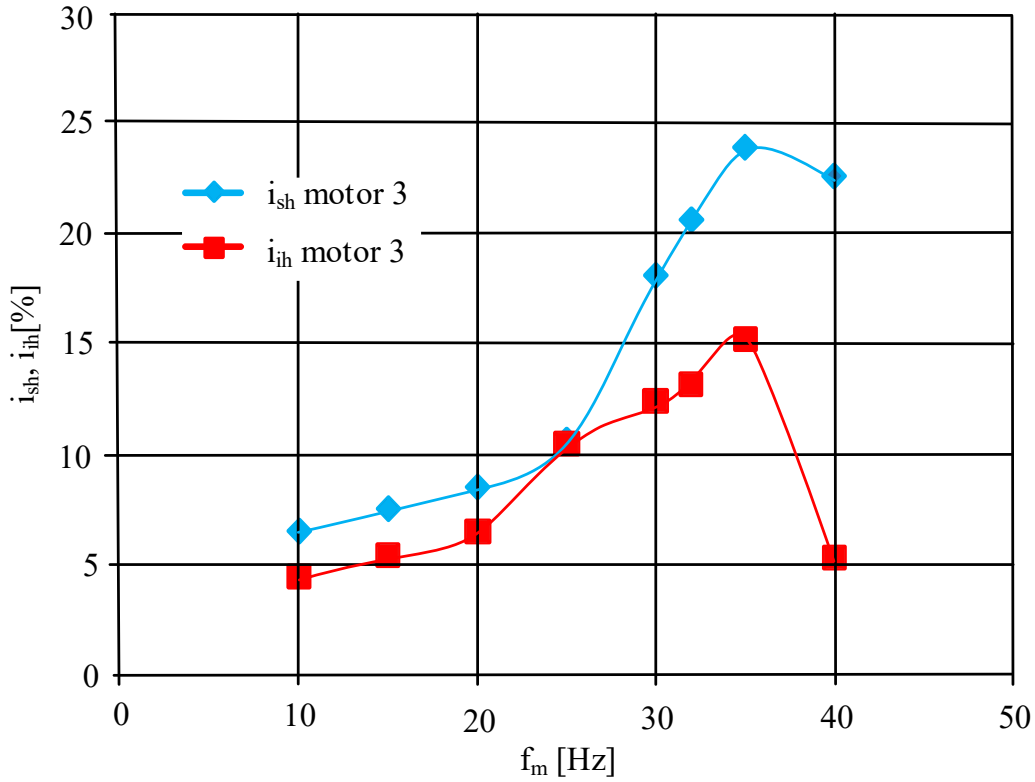

Figure 23. Measured current subharmonics and interharmonics versus the frequency of the amplitude modulation for Case B. The frequency components are related to the rated current.

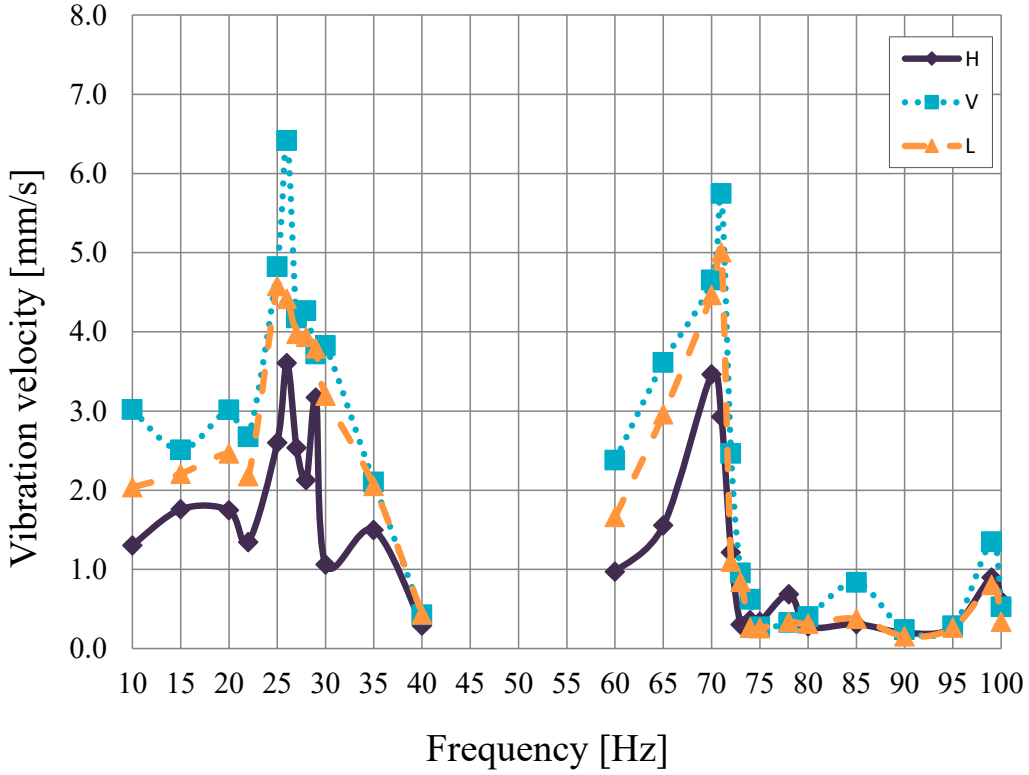

Figure 24. Measured broad-band vibration velocity for Case A in the horizontal (H), vertical (V) and longitudinal (L) directions versus the frequency of voltage subharmonics and interharmonics occurring as a single power quality disturbance.

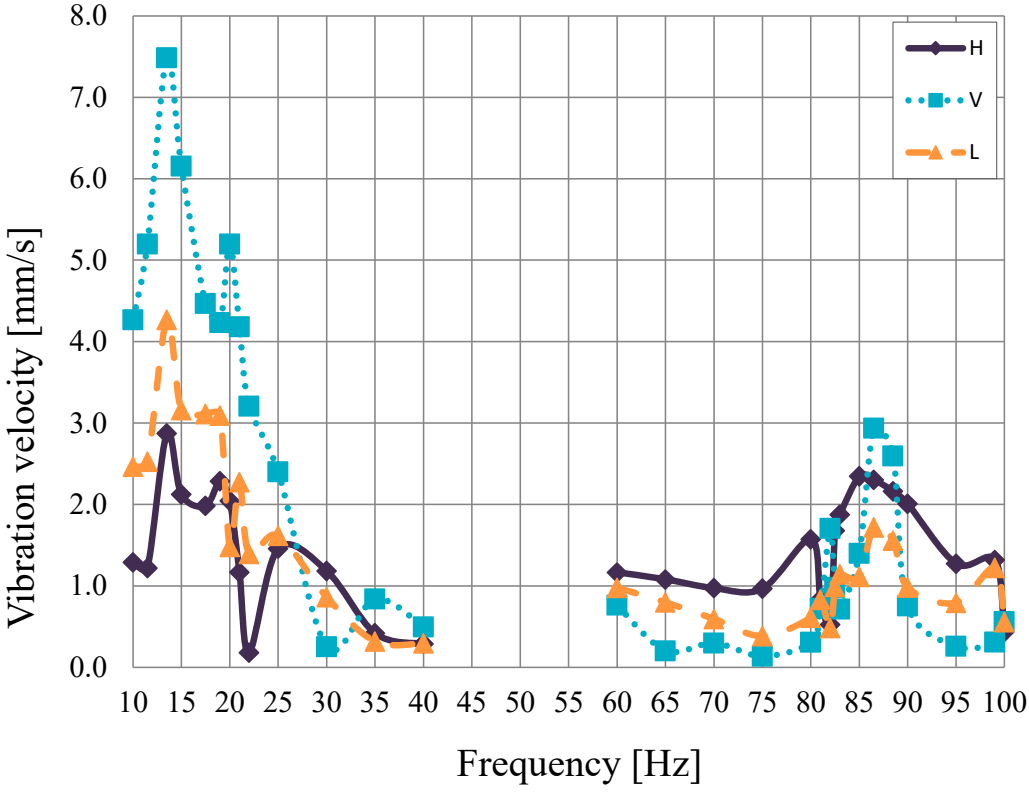

Figure 25. Measured broad-band vibration velocity for Case B in the horizontal (H), vertical (V) and longitudinal (L) directions versus the frequency of voltage subharmonics and interharmonics occurring as a single power quality disturbance.

8. Conclusions

Periodical voltage fluctuations can be regarded as the superposition of symmetrical voltage subharmonics and interharmonics (*SSaIs*). Depending on their phase angles, the following can be distinguished: amplitude modulation (*AM*), phase modulation (*PhM*) and intermediate cases. At the same time, voltage fluctuations are usually considered as the perfect amplitude modulation (based on [42]). This approach apparently seems justified, as the phase modulation has rather a little effect on light flickers (based on [22]), which are believed to be a particularly serious problem caused by voltage fluctuations. In fact, rotating machinery is especially susceptible to voltage fluctuations (or voltage subharmonics and interharmonics). Voltage fluctuations (e.g., in the output voltage in an inverter) may even lead to a mechanical failure of a power train [12,20].

In this study, noxious phenomena occurring in induction motors under *SSaIs* were analyzed taking into account their phase angles. The presented results of the research show that in some cases phase angles are almost as important as the value of voltage *SSaIs*. For some phase angles, the torque pulsations could be even about ten times greater than for other phase angles. It should be stressed that for some motors the most harmful effect of voltage *SSaIs* occurs for the phase angles approximately corresponding to the *PhM*, and the least detrimental for the phase angles corresponding to the *AM*. Consequently, from the point of view of induction motors, voltage fluctuations cannot be a priori considered as the perfect *AM*. This approach may lead to a significant underestimation of the effect of voltage fluctuations on induction motors.

Further, the most significant effect of phase angles on undesirable phenomena due to *SSaIs* was observed for motor1 (of the rated power 200 kW), while for motor2 (3 kW) it was less considerable. It was also found that voltage fluctuations may result in vibration, the velocity of which is normally considered to be of sufficient severity to cause damage to the machine [45]. Under the *AM*, the measured vibration velocity was comparable with its value caused by a single subharmonic injection.

The presented results of the investigations lead to two practical conclusions. Firstly, during the analysis of an induction motor under *SSaIs* of unknown phase angles, a safe approach is to assume such phase angles for which the torque pulsations are caused separately by voltage subharmonics and voltage interharmonics add up algebraically. Secondly, the power quality standards (PQSs) should not contain only the limits for single voltage subharmonics and interharmonics. They should also take into account the cumulative effect of voltage *SSaIs*; in practice, separate limits for single-voltage subharmonics, interharmonics and *SSaIs* could be included in the standards. The elaboration of a proposal for *PQSs* modification will be the subject of future research work.

Author Contributions: Conceptualization, P.G., D.H. and M.P.; methodology, D.H., P.K. and M.P.; formal analysis, D.H, P.K., A.M. and M.P.; investigation D.H, P.K., A.M. and M.P.; writing—original draft preparation, P.G.; supervision, P.G. All authors have read and agreed to the published version of the manuscript.

Funding: This project is financially supported under the framework of a program of the Ministry of Science and Higher Education (Poland) as "Regional Excellence Initiative" in the years 2019–2022, project number 006/RID/2018/19, amount of funding 11 870 000 PLN.

Data Availability Statement: Not applicable.

Conflicts of Interest: The authors declare no conflict of interest. The funders had no role in the design of the study; in the collection, analyses, or interpretation of data; in the writing of the manuscript; or in the decision to publish the results.

References

1. Nandi, S.; Toliyat, H.A.; Li, X. Condition monitoring and fault diagnosis of electrical motors—A review. *IEEE Trans. Energy Convers.* **2007**, *20*, 719–729. [CrossRef]
2. Tsypkin, M. Induction motor condition monitoring: Vibration analysis technique—Diagnosis of electromagnetic anomalies. In Proceedings of the 2017 IEEE International Automatic Testing Conference, Schaumburg, IL, USA, 9–15 September 2017.
3. Tsypkin, M. The origin of the electromagnetic vibration of induction motors operating in modern industry: Practical experience—Analysis and diagnostics. *IEEE Trans. Ind. Appl.* **2017**, *53*, 1669–1676. [CrossRef]
4. Crotti, G.; D'Avanzo, G.; Letizia, P.S.; Luiso, M. Measuring harmonics with inductive voltage transformers in presence of subharmonics. *IEEE Trans. Instrum. Meas.* **2021**, *70*, 9005013. [CrossRef]
5. Gnacinski, P.; Peplinski, M.; Murawski, L.; Szelezinski, A. Vibration of induction machine supplied with voltage containing subharmonics and interharmonics. *IEEE Trans. Energy Convers.* **2019**, *34*, 1928–1937. [CrossRef]
6. Jardan, R.K.; Stumpf, P.; Bartal, P.; Varga, Z.; Nagy, I. A novel approach in studying the effects of subharmonics on ultrahigh-speed ac motor drives. *IEEE Trans. Ind. Electron.* **2010**, *58*, 1274–1281. [CrossRef]
7. Zhang, S.; Kang, J.; Yuan, J. Analysis and suppression of oscillation in V/F controlled induction motor drive systems. *IEEE Trans. Transp. Electrif.* **2022**, *8*, 1566–1574. [CrossRef]
8. Bollen, M.H.J.; Gu, I.Y.H. Origin of Power Quality Variations. Processing of Stationary Signals. In *Signal Processing of Power Quality Disturbances*; Wiley: New York, NY, USA, 2006; pp. 41–276.
9. Arkkio, A.; Cederström, S.; Awan, H.A.A.; Saarakkala, S.E.; Holopainen, T.P. Additional losses of electrical machines under torsional vibration. *IEEE Trans. Energy Convers.* **2018**, *33*, 245–251. [CrossRef]
10. Avdeev, B.A.; Vyngra, A.V.; Chernyi, S.G.; Zhilenkov, A.A.; Sokolov, S.S. Evaluation and procedure for estimation of inter-harmonics on the example of non-sinusoidal current of an induction motor with variable periodic load. *IEEE Access* **2021**, *9*, 158412–158419. [CrossRef]
11. Nassif, A.B. Assessing the impact of harmonics and interharmonics of top and mudpump variable frequency drives in drilling rigs. *IEEE Trans. Ind. Appl.* **2019**, *55*, 5574–5583. [CrossRef]
12. Schramm, S.; Sihler, C.; Song-Manguelle, J.; Rotondo, P. Damping torsional interharmonic effects of large drives. *IEEE Trans. Power Electron.* **2010**, *25*, 1090–1098. [CrossRef]
13. Soltani, H.; Davari, P.; Zare, F.; Blaabjerg, F. Effects of modulation techniques on the input current interharmonics of adjustable speed drives. *IEEE Trans. Ind. Electron.* **2018**, *65*, 167–178. [CrossRef]
14. Testa, A.; Akram, M.F.; Burch, R.; Carpinelli, G.; Chang, G.; Dinavahi, V.; Hatziadoniu, C.; Grady, W.M.; Gunther, E.; Halpin, M.; et al. Interharmonics: Theory and modeling. *IEEE Trans. Power Deliv.* **2007**, *22*, 2335–2348. [CrossRef]
15. Zhang, D.; Xu, W.; Liu, Y. On the phase sequence characteristics of interharmonics. *IEEE Trans. Power Deliv.* **2005**, *20*, 2563–2569. [CrossRef]
16. Chang, G.W.; Lin, Y.L.; Liu, Y.J.; Sun, G.H.; Yu, J.T. A hybrid approach for time-varying harmonic and interharmonic detection using synchrosqueezing wavelet transform. *Appl. Sci.* **2021**, *11*, 752. [CrossRef]
17. Ravindran, V.; Busatto, T.; Rönnberg, S.K.; Meyer, J.; Bollen, M.H. Time-varying interharmonics in different types of grid-tied PV inverter systems. *IEEE Trans. Power Deliv.* **2019**, *35*, 483–496. [CrossRef]
18. Xie, X.; Zhang, X.; Liu, H.; Liu, H.; Li, Y.; Zhang, C. Characteristic analysis of subsynchronous resonance in practical wind farms connected to series-compensated transmissions. *IEEE Trans. Energy Convers.* **2017**, *32*, 1117–1126. [CrossRef]
19. Zhong, Q.; Qiu, Y.; Zhao, Y.; Li, H.; Wang, G.; Wen, F. Interharmonic analysis model of photovoltaic grid-connected system with extended dynamic phasors. *J. Mod. Power Syst. Clean Energy* **2021**, *9*, 1540–1547. [CrossRef]
20. Tripp, H.; Kim, D.; Whitney, R. A comprehensive cause analysis of a coupling failure induced by torsional oscillations in a variable speed motor. In *Proceedings of the 22nd Turbomachinery Symposium*; Texas A&M University, Turbomachinery Laboratories: College Station, TX, USA, 1993; pp. 17–24.
21. Barros, J.; de Apraiz, M.; Diego, R.I. Measurement of subharmonics in power voltages. In Proceedings of the Power Tech 2007 IEEE Conference, Lausanne, Switzerland, 1–5 July 2007; pp. 1736–1740.
22. Gallo, D.; Landi, C.; Langella, R.; Testa, A. Limits for low frequency interharmonic voltages: Can they be based on the flickermeter use. In Proceedings of the 2005 IEEE Russia Power Tech, St. Petersburg, Russia, 27–30 June 2005; pp. 1–7.
23. Ghaseminezhad, M.; Doroudi, A.; Hosseinian, S.H.; Jalilian, A. High torque and excessive vibration on the induction motors under special voltage fluctuation conditions. *COMPEL—Int. J. Comput. Math. Electr. Electron. Eng.* **2021**, *40*, 822–836. [CrossRef]
24. Tennakoon, S. Flicker Propagation in Radial and Interconnected Power Systems. Ph.D. Dissertation, School of Electrical, Computer and Telecommunications Engineering, University of Wollongong, Wollongong, Australia, 2008.
25. Tennakoon, S.; Perera, S.; Robinson, D. Flicker attenuation—Part I: Response of three-phase induction motors to regular voltage fluctuations. *IEEE Trans. Power Deliv.* **2008**, *23*, 1207–1214. [CrossRef]
26. Gnaciński, P.; Muc, A.; Pepliński, M. Influence of voltage subharmonics on line start permanent magnet synchronous motor. *IEEE Access* **2021**, *9*, 164275–164281. [CrossRef]
27. Ghaseminezhad, M.; Doroudi, A.; Hosseinian, S.H.; Jalilian, A. Analysis of voltage fluctuation impact on induction motors by an innovative equivalent circuit considering the speed changes. *IET Gener. Transm. Distrib.* **2017**, *11*, 512–519. [CrossRef]
28. Ghaseminezhad, M.; Doroudi, A.; Hosseinian, S.H.; Jalilian, A. An investigation of induction motor saturation under voltage fluctuation conditions. *J. Magn.* **2017**, *22*, 306–314. [CrossRef]

29. Ghaseminezhad, M.; Doroudi, A.; Hosseinian, S.H.; Jalilian, A. Analytical field study on induction motors under fluctuated voltages. *Iran. J. Electr. Electron. Eng.* **2021**, *17*, 1620.
30. Ghaseminezhad, M.; Doroudi, A.; Hosseinian, S.H.; Jalilian, A. Investigation of increased ohmic and core losses in induction motors under voltage fluctuation conditions. *Iran. J. Sci. Technol. Trans. Electr. Eng.* **2018**, *43*, 373–382. [CrossRef]
31. Gnaciński, P.; Hallmann, D.; Klimczak, P.; Muc, A.; Pepliński, M. Effects of voltage interharmonics on cage induction motors. *Energies* **2021**, *14*, 1218. [CrossRef]
32. Gnacinski, P.; Klimczak, P. High-Power induction motors supplied with voltage containing subharmonics. *Energies* **2020**, *13*, 5894. [CrossRef]
33. Gnaciński, P.; Pepliński, M.; Hallmann, D.; Jankowski, P. Induction cage machine thermal transients under lowered voltage quality. *IET Electr. Power Appl.* **2019**, *13*, 479–486. [CrossRef]
34. Gnacinski, P.; Peplinski, M.; Hallmann, D.; Jankowski, P. The effects of voltage subharmonics on cage induction machine. *Int. J. Electr. Power Energy Syst.* **2019**, *111*, 125–131. [CrossRef]
35. Zhao, K.; Cheng, L.; Zhang, C.; Nie, D.; Cai, W. Induction motors lifetime expectancy analysis subject to regular voltage fluctuations. In Proceedings of the 2017 IEEE Electrical Power and Energy Conference (EPEC), Saskatoon, SK, Canada, 22–25 October 2017.
36. Feese, T.; Ryan, M. Torsional vibration problem with motor/ID fan system due to PWM variable frequency drive. In *Proceedings of the 37th Turbomachinery Symposium*; Texas A&M University, Turbomachinery Laboratories: College Station, TX, USA, 2008; pp. 45–56.
37. *aEN Standard 50160*; Voltage Characteristics of Electricity Supplied by Public Distribution Network. CELENEC: Brussels, Belgium, 2010.
38. *IEEE Standard 519-2014 (Revision of IEEE Standard 519-1992)*; IEEE Recommended Practice and Requirements for harmonic Control in Electric Power Systems. IEEE: New York, NY, USA, 2014.
39. Tarasiuk, T.; Jayasinghe, S.G.; Gorniak, M.; Piłat, A.; Shagar, V.; Liu, W.; Guerrero, J.M. Review of power quality issues in maritime microgrids. *IEEE Access* **2021**, *9*, 81798–81817. [CrossRef]
40. Kuwałek, P. Selective identification and localization of voltage fluctuation sources in power grids. *Energies* **2021**, *14*, 6585. [CrossRef]
41. Patel, D.; Chowdhury, A. Mitigation of voltage fluctuation in distribution system using Sen transformer with variable loading conditions. In Proceedings of the 2021 International Conference on Advances in Electrical, Computing, Communication and Sustainable Technologies (ICAECT), Bhilai, India, 19–20 February 2021; pp. 1–6.
42. Kuwalek, P. Estimation of parameters associated with individual sources of voltage fluctuations. *IEEE Trans. Power Deliv.* **2021**, *36*, 351–361. [CrossRef]
43. *IEEE/IEC Standard 60255-118-1-2018*; Measuring Relays and Protection Equipment—Part 118-1: Synchrophasor for Power Systems—Measurements. IEEE: New York, NY, USA, 2018.
44. *IEC Standard IEC61000-4-7*; Electromagnetic Compatibility (EMC)—Part 4–7: Testing and Measurement Techniques—General Guide on Harmonics and Interharmonics Measurements and Instrumentation, for Power Supply Systems and Equipment Connected Thereto. International Electrotechnical Commission: Geneva, Switzerland, 2002.
45. *ISO Standard 20816-1*; Mechanical Vibration—Measurement and Evaluation of Machine Vibration—Part 1: General Guidelines. ISO: Genova, Switzerland, 2016.
46. *ISO Standard 10816-1*; Mechanical Vibration—Evaluation of Machine Vibration by Measurements on Non-Rotating Parts—Part 1: General Guidelines. ISO: Genova, Switzerland, 1995.
47. Gulbudak, O.; Gokdag, M.; Komurcugil, H. Model predictive control strategy for induction motor drive using Lyapunov stability objective. *IEEE Trans. Ind. Electron.* **2022**, *69*, 12119–12128. [CrossRef]
48. Lucas, G.B.; de Castro, B.A.; Rocha, M.A.; Andreoli, A.L. Three-phase induction motor loading estimation based on Wavelet Transform and low-cost piezoelectric sensors. *Measurement* **2020**, *164*, 107956. [CrossRef]
49. Wengerkievicz, C.A.; Elias, R.D.A.; Batistela, N.J.; Sadowski, N.; Kuo-Peng, P.; Lima, S.C.; Silva, P.A.D.; Beltrame, A.Y. Estimation of three-phase induction motor equivalent circuit parameters from manufacturer catalog data. *J. Microw. Optoelectron. Electromagn. Appl.* **2017**, *16*, 90–107. [CrossRef]
50. *IEC Standard 60034-1*; Rotating Electrical Machines. Part 1: Rating and Performance. IEC: Genova, Switzerland, 2004.